KINETICS OF DEFORMATION-INDUCED TRANSFORMATION OF DISPERSED AUSTENITE IN TWO ALLOY SYSTEMS

by

YUKIO KURODA

B.E., Metallurgy, Tohoku University (1977)
M.E., Metallurgy, Tohoku University (1980)

Submitted to the Department of
Materials Science and Engineering
in Partial Fulfillment of the Requirements for the Degree of

MASTER OF SCIENCE

at the

MASSACHUSETTS INSTITUTE OF TECHNOLOGY
June, 1987
© Massachusetts Institute of Technology, 1987

Signature of Author _____
Department of Materials Science and Engineering
May 8, 1987

Certified by _____
Morris Cohen
Institute Professor Emeritus
Thesis Supervisor

Certified by _____
Dr. Gregory B. Olson
Senior Research Associate
Thesis Supervisor

Accepted by _____
Samuel M. Allen
Chairman, Departmental Committee on Graduate Students

MASSACHUSETTS INSTITUTE OF TECHNOLOGY
JUN 22 1987
LIBRARIES
Archives

KINETICS OF DEFORMATION-INDUCED TRANSFORMATION OF DISPERSED AUSTENITE IN TWO ALLOY SYSTEMS

by

Yukio KURODA

Submitted to the Department of Materials Science and Engineering on May 8, 1987 in partial fulfillment of the requirements for the Degree of Master of Science

Abstract

A simple model for expressing the kinetics of deformation-induced transformation of dispersed austenite has been developed by following the defect dissociation model and assuming an exponential distribution function of cumulative structural defects. The model was applied to the deformation-induced transformation of isolated austenitic iron particles in the Cu-Fe single crystal and has predicted transformation behavior and the smallest size of transformable particles well. The model was also applied to the transformation of retained austenite in the dual phase steel. Transformation behavior in the early stage of

deformation and the significant contribution from the stress-assisted nucleation have been well accounted.

Thesis Supervisor : Dr. Morris Cohen
Title : Institute Professor, Emeritus

Thesis Supervisor : Dr. Gregory B. Olson
Title : Senior Research Associate

Table of Contents

Title Page....1
Abstract....2
Table of Contents....4
List of Figures....6
List of Tables....10
Acknowledgements....11
1. Introduction....13
2. Review of the Recent Models....16
2-1. Stress-assisted Nucleation....16
2-2. Strain-induced Nucleation....20
3. A Simple Model for Kinetics of Deformation-Induced Transformation in Dispersed Austenite....22
3-1. Potency Distribution in Dispersed Particles under Deformation....22
3-2. Kinetics of Deformation-Induced Transformation....25
4. Analysis of Transformation Behavior in the Cu-Fe System....26
4-1. Review of the Data....26
4-2. Estimation of Parameters....32
4-3. Prediction of Transformation Behavior....53
5. Application of the Model to a "Dual-Phase" Steel....60
5-1. Review of the Data....60
5-2. Estimation of Parameters....64
5-2-1. Estimation of average volume of retained austenite and stress-strain relations....64
5-2-2. Estimation of effects of alloying elements on stability of retained austenite....65
5-2-2-1. Chemical effects....65
5-2-2-2. Mechanical effects....67
5-2-3. Contribution of stress-assisted nucleation....74
5-3. Prediction of Transformation Behavior....76
6. Discussion....80

6-1. On the Model....80
6-2. On the Cu-Fe System....81
6-2-1. Effect of stress-assisted transformation....81
6-2-2. Prediction of the smallest size of transformed particles....81
6-3. On the Dual-Phase Steel....86
7. Conclusions....87
8. Bibliography....89

List of Figures

Fig.1-a Change in the fraction of transformed austenitic iron particles in the Cu-Fe alloy single crystal with particle size at 77K for several tensile strains p.28

Fig.1-b Change in the fraction of transformed austenitic iron particles in the Cu-Fe alloy single crystal with particle size at 200K for several tensile strains p.29

Fig.2-a Change in the fraction of transformed austenitic iron particles in the Cu-Fe alloy single crystal with tensile strain for several particle sizes at 77K p.30

Fig.2-b Change in the fraction of transformed austenitic iron particles in the Cu-Fe alloy single crystal with tensile strain for several particle sizes at 200K p.31

Fig.3-a Determination of the site for nucleation, i.e., volume nucleation or surface nucleation, in austenitic iron particles at 200K p.35

Fig.3-b Determination of the site for nucleation, i.e., volume nucleation or surface nucleation, in austenitic iron particles at 200K p.36

Fig.4-a Best fit of the deformation-induced transformation behavior of austenitic iron particles the Cu-Fe alloy single crystal at 77K by the equation, $f=1-\exp(-NvVp)$ p.37

Fig.4-b Best fit of the deformation-induced transformation behavior of austenitic iron particles the Cu-Fe alloy single crystal at 200K by the equation, $f=1-\exp(-NvVp)$ p.38

Fig.5 Change in the number density of nucleation sites with true plastic strain for several temperatures p.39

Fig.6 Change in the number density of nucleation sites created by plastic strain through strain-induced nucleation p.46

Fig.7 Tensile stress-strain relations of the Cu-Fe alloy single crystal containing austenitic iron particles having the average diameter of 30nm for several temperatures p.47

Fig.8 Tensile stress-strain relations of the Cu-Fe alloy single crystal containing austenitic iron particles having the average diameter of 106nm for several temperatures p.48

Fig.9 Change in the number density of nucleation sites with the number of atomic planes in a defect for the strain-induced nucleation p.49

Fig.10 Determination of the distribution shape factor for strain-induced nucleation, an absolute value of the slope is the distribution shape factor p.50

Fig.11 Change in the total number of nucleation sites of all potencies with true plastic strain for strain-induced nucleation p.51

Fig.12 Prediction of the change in the total number of nucleation sites of all potencies with true plastic strain for strain-induced nucleation p.52

Fig.13 Prediction of the variation of the number density of nucleation sites with strain from the kinetic model p.54

Fig.14-a Prediction of the deformation-induced transformation behavior of austenitic iron particles in the Cu-Fe alloy single crystal with particle diameter for several tensile strains at 77K p.55

Fig.14-b Prediction of the deformation-induced transformation behavior of austenitic iron particles in the Cu-Fe alloy single crystal with particle diameter for several tensile strains at 200K p.56

Fig.15-a Prediction of the change in the fraction of deformation-induced transformation behavior of austenitic iron particles in the Cu-Fe alloy single crystal with strain for several particle sizes at 77K p.57

Fig.15-b Prediction of the change in the fraction of deformation-induced transformation behavior of austenitic iron particles in the Cu-Fe alloy single crystal with strain for several particle sizes at 200K p.58

Fig.15-c Prediction of the change in the fraction of deformation-induced transformation behavior of austenitic iron particles in the Cu-Fe alloy single crystal with strain at 300K p.59

Fig.16 Variation of the fraction of transformed retained austenite in the dual phase steel with true plastic strain p.62

Fig.17 Variation of the volume fraction of martensite transformed from the retained austenite in the dual phase steel with true plastic strain p.63

Fig.18 Composition dependence of the frictional work of interfacial motion (Fe-Mn-Ni alloy) p.72

Fig.19 Composition dependence of the frictional work of interfacial motion (Fe-C alloy) p.73

Fig.20 Best fit of the deformation-induced transformation behavior of retained austenite with true plastic strain, using the model and estimating $N_v^{\circ\circ}$ and $DG=g^{ch}+g_{el}+W_f$. p.78

Fig.21 Effects of the chemical composition on austenite stabilization p.79

Fig.22 Determinaion of the distribution shape factor for stress-assisted nucleation in the zirconia-containing ceramics p.83

Fig.23-a Comparison of the temperature and strain depenence of the smallest size of transformed particles between experiments and predictions (f=0.01) p.84

Fig.23-b Comparison of the temperature and strain depenence of the smallest size of transformed particles between experiments and predictions (f=0.05) p.85

List of Tables

Table1. Values of $N_{\underline{v}}$ p.34

Table 2. Nv-Nv(stress) and Nv° p.45

Table 3. Properties of the dual phase steel p.61

Acknowlegements

The author wishes to express his sincere appreciation to the follwing people for their assistance in conducting the work reported in this thesis :

Professor Morris Cohen for giving a special chance to study Martensitic Transformation and to understand important things in a human life as a graduate student in his faculty ;

Dr. Gregory B. Olson for guiding this study with his ideas and suggestions and provoking my thought not only about my study but also the future of steel research ;

Ms Marge Meyer for her patience and warm heart in understanding a person's heart and soul and for her invaluable help to many people, especially from Japan ;

Professor Samuel M. Allen for giving a number of suggestions not only on the course subject but also on my research ;

Sam, his wife Jeannie, Anna, and Micah for their kind and heart-warming invitation ;

Dr. John F. Watton for showing his marvelous accomplishment and making me think about a importance of life and family. He was very patient with my poor English, which made me feel really comfortable in the office.

Mr. Chune-Ching Young for giving uncountable suggestions and assistance necessary for surviving at MIT.

We spent a lot of time, mostly on weekends and at nights, to talk about everything and this helped me to find the roots of my mind and personality.

Mr. Jenh-Yih Juang for supporting my survival at several courses and sharing our time at the pub, on the tennis court, and in the office which made my life at MIT pleasant ;

Drs. Mica Grujicic, Dennis Haezebrouck, Yutaka Hara, Matthew Libera, and Yuh Shiohara, and fellow students Mark A. Buonanno, Gary M. Carinci, Mark J. Gore, Gregory Heidemenopoulos, Minfa Lin, Shin-ichi Sasayama, and Frode Stavehaug for their friendship, assistance, and stimulating conversation.

1. Introduction

Phase transformation of crystalline materials is generally accompanied by transformation strains and a local change in elastic constants. Deformation can affect the kinetics of such phase transformations through both the thermodynamic effect of stress and the production of new catalyzing defects by plastic strain.

For martensitic transformation under an applied stress, a remarkable increase in both uniform elongation and ultimate tensile strength has been obtained[1] and this phenomenon is called TRansformation Induced Plasticity, (TRIP). This occurs not only in ferrous martensite but also in non-ferrous materials such as Cu-Zn and Ti-Al-Co[2], and has been commonly utilized to improve mechanical properties of austenitic stainless steels. Recently, it has been observed that transformation plasticity can play an important role in the deformation of materials with dispersed metastable austenitic particles such as "dual phase" steels[3,4] and partially stabilized zirconia, and this provides a new possibility for developing high strength materials.

The effect of deformation on martensitic nucleation kinetics has been classified into two types according to the

difference in mechanism through which the deformation affects the nucleation. Heterogeneous nucleation on the same sites responsible for transformation on cooling but assisted by stress is termed stress-assisted, whereas nucleation on new sites produced by plastic strain is termed strain-induced[5].

It has been well established that the essential mechanism of heterogeneous martensitic nucleation is the same for both stress-assisted and strain-induced cases[6,7]. The potency distribution of nucleation sites controlling the transformation under cooling has been derived by Cohen and Olson[8] based on the classical small-particle experiments of Cech and Turnbull[9]. In the case of stress-assisted nucleation, applied elastic stress assists the transformation kinetics by modifying the effective thermodynamic potency distribution of nucleation sites. Olson and Tsuzaki[10,11] have analyzed the effect of stress and the form of potency distribution statistically by using the results of Cohen and Olson[9]. They successfully estimated the distribution and predicted the transformation plasticity in composite materials containing metastable dispersed austenite, and the transformation yield locus for multi-axial stress.

The kinetics of strain-induced nucleation in an uniform austenite phase has been treated by Olson and Cohen[12] by assuming that shear-band intersections are the dominant nucleation sites. They have derived an expression theoretically relating the volume fraction of martensite to plastic strain and obtained good agreement between their model and the experimental results of Angel[13]. However, kinetics of strain-induced nucleation in dispersed austenite particles has not been studied, although this can be very important in the practical applications of transformation plasticity to improve the ductility and toughness of high-strength steels.

In this study, a simple model will be developed for the deformation induced martensitic transformation of dispersed austenite particles in model Cu-Fe alloys with special emphasis on the strain-induced nucleation, assuming the same type of potency distribution of nuclei as used in the analysis of stress-assisted nucleation. The model will then be applied to the more complex system of a "dual-phase" steel to predict the martensitic transformation of retained austenite particles induced by tensile deformation.

2. Review of the Recent Models

As mentioned in the introduction, the effects of applied stress on martensitic nucleation have been treated quantitatively since Cohen and Olson[9] first introduced the idea of simple defect dissociation model. In this section, previous analysis on the kinetics of both stress-assisted and strain-induced transformation will be briefly reviewed.

2-1. Stress-assisted Nucleation

According to the general faulting mechanism[14,15] by which the major lattice change occurring in martensitic transformations can be derived from an appropriate group of dislocations, the total free energy of a martensitic embryo can be separated into dislocation energy and fault energy, with the fault energy $\gamma(n)$ per unit area in the defect plane given by :

$$\gamma(n) = n\,d\left[\Delta g^{ch} + g_{el}\right] + 2\,\gamma_s \qquad (1)$$

where γ_s is the nucleus specific interfacial energy, d is the close-packed interplanar spacing, and g_{el} is an elastic coherency strain energy associated with distortions in the nucleus interface plane. When Δg^{ch} is greater in magnitude than g_{el}, then the defect energy becomes smaller with increasing thickness such that for some critical value of n,

$\gamma(n)$ may be zero or negative. Under these conditions, a group of dislocations which can produce a defect of critical thickness will become unstable and spontaneous nucleation will occur. The size of the defect necessary to account for spontaneous embryo formation can be obtained by regarding the critical condition as $\gamma(n)=-ndW_f$ where W_f is the frictional work of interfacial motion. This gives the condition :

$$n = -\left[\frac{2\gamma_s / d}{\Delta g^{ch} + g_{el} + w_f}\right] \qquad (2)$$

Based on this model, Cohen and Olson[9] derived theoretically a cumulative structural defect potency distribution $N_v(n)$ consistent with the Cech-Turnbull small particle experiments in Fe-30at%Ni[10] :

$$N_v(n) = N_v^o \exp(-\alpha n) \qquad (3)$$

where α is a constant distribution shape factor and N_v^o is the total number density of nucleation sites of all potencies. The form of this equation is typical of experimentally observed distribution functions for sparsely distributed nonequilibrium structural defects as encountered in fracture and fatigue. Recent observations of nucleation at well-

characterized low potency defects in small particles of ZrO_2 ceramics[16] have confirmed the generality of this equation. The statistics of transformation behavior in the ZrO_2 particles is found to conform to the same form of distribution function as the Cech-Turnbull experiment. Combining Eq.(2) and (3), a thermodynamic potency distribution Nv(Δg) can be expressed as :

$$N_v(\Delta g) = N_v^o \exp\left[\frac{2\alpha\gamma_s / d}{\Delta g^{ch} + g_{el} + w_f}\right] \qquad (4)$$

When martensitic transformation occurs under an applied stress as originally treated by Patel and Cohen[17], the total volume free-energy change or "driving force" for transformation should be the sum of a chemical term, Δg^{ch}, and a mechanical contribution, Δg^{σ}. The Δg^{σ} term is orientation dependent and for a uniaxial stress, σ, can be expressed by :

$$\Delta g^{\sigma} = -\frac{\sigma}{2}\left[\gamma_o \sin 2\theta \cos\alpha + \varepsilon_o(1+\cos 2\theta)\right] \qquad (5)$$

where γ_o and ε_o are the transformation shear and normal strains, θ is the angle between the stress axis and the habit normal, and α is the angle between the transformation shear

direction and the maximum shear stress direction resolved on the habit. The value of Δg^{σ} is in the range from Δg^{σ}_{min} to Δg^{σ}_{max} given by :

$$\Delta g^{\sigma}_{min} = -\frac{1}{2}\left[-|\sigma|\sqrt{\gamma_o^2 + \varepsilon_o^2} + \sigma\varepsilon_o \right] \quad \text{and} \quad \Delta g^{\sigma}_{max} = -\frac{1}{2}\left[|\sigma|\sqrt{\gamma_o^2 + \varepsilon_o^2} + \sigma\varepsilon_o \right] \tag{6}$$

Olson and Tsuzaki[11,12] have calculated the mechanical driving force distribution from this expression by changing θ and α to give certain values of Δg^{σ} and then obtained a modified potency distribution of randomly oriented nucleation sites under uniaxial tension and compression. Their results have showed that in the stress-assisted regime, the effect of applied stress was approximately one-third of that predicted by the assumption that all operational nuclei have the optimum orientation. In other words, the modified potency distribution under an applied elastic stress can be estimated by letting $\Delta g^{\sigma} = \Delta g^{\sigma}_{max}/3$. Therefore, the distribution is given by :

$$N_v(\sigma) = N_v^o \exp\left[\frac{2\,\alpha\,\gamma_s / d}{\Delta g^{ch} + (\Delta g^{\sigma}_{max}/3) + g_{el} + w_f} \right] \tag{7}$$

Olson and Tsuzaki[11,12] gave estimated values of some of the parameters in the above equation as : α=0.84, γ_s=0.15 J/m^2, d=2x10^{-10} m, $g_{\theta l}+w_f$=6.1x10^7 J/m^3 and N_v°=2x10^{17} m^{-3}.

2-2. Strain-induced Nucleation

A quantitative model for the sigmoidal transformation behavior in steels with an uniform austenite phase has been developed by Olson and Cohen. They assumed that shear-band intersections constitute the primary strain-induced nucleation sites and the volume fraction of shear bands are related to plastic strain by an equation of the form :

$$f^{sb} = 1 - \exp (- \alpha \varepsilon) \tag{8}$$

where the rate of shear band formation is determined by a single dimensionless parameter. For an average shear band volume v^{sb}, the number of shear bands per unit volume N_v^{sb} is f^{sb}/v^{sb}. The number of intersections N_v^I is assumed to be related to N_v^{sb} by a simple power law :

$$N_v^I = K (N_v^{sb})^n \tag{9}$$

where K is a geometric constant and n $\geq$ 2. The number of martensitic units $N_v^{\alpha'}$ of average volume $V^{\alpha'}$ is related to N_v^I

by the probability p that an intersection will act as a nucleation site :

$$d N_v^{\alpha'} = p \; d N_v^{I} \tag{10}$$

These assumptions lead to an expression for the volume fraction of strain-induced martensite as a function of plastic strain of the form :

$$f^{\alpha'} = 1 - \exp\left[- \beta \{ 1 - \exp (- \alpha \varepsilon) \}^n \right] \quad \text{where} \quad \beta = p \left[\frac{v^{\alpha'} K}{(v^{sb})^n} \right] \tag{11}$$

This model accounted quite well for the sigmoidal transformation behavior of an uniform austenite phase. However, applicability of this model to austenite as a dispersed phase seems to be questionable since this model has simply assumed a Gaussian distribution of nucleation site potency and assigned some adjustable parameters instead of having taken into account the effects of an applied stress and stability of austenite explicitly and obtaining the form of the operative potency distribution.

3. A Simple Model for Kinetics of Deformation-Induced Transformation in Dispersed Austenite

3-1. Potency Distribution in Dispersed Particles under Deformation

In the stress-assisted region, the same type of potency distribution developed by Olson and Tsuzaki[11,12] can be applied. The total number of nucleation sites of all potencies may not be same since the nature of austenite phase is completely different in the present case. The potency distribution in the stress-assisted regime will be expressed as :

$$N_v(\sigma) = N_v^o \exp\left[\frac{2\alpha\gamma_s / d}{\Delta g^{ch} + (\Delta g^{\sigma}_{max} / 3) + g_{el} + w_f}\right] \qquad (12)$$

In the strain-induced regime, the potency distribution can be treated in two different ways, namely to follow the same way as in the analysis of an uniform austenite phase and assume Gaussian distribution or to apply the same type of exponential distribution as applied in stress-assisted regime. However, as stated in the previous chapter, the former way is not applicable for dispersed particles. Therefore, the latter way will be followed.

In the strain-induced regime, the mechanical contribution of an applied stress Δg^{σ} has basically the same form as Eq.(5). However, since new nucleation sites are created by plastic strain in a certain direction in this regime, it is not unreasonable to assume that those new nucleating defects will have a preferred orientation which is very close to the optimum one. That is, new defects are produced in such a way that the work done by the applied stress is nearly maximum for their orientation variant. This implies that the potency distribution in the strain-induced region can be approximated by using $\Delta g^{\sigma}=\Delta g^{\sigma}_{max}$. Therefore, the distribution is expressed by :

$$N_v(\varepsilon) = N_v^{o}(e)\exp\left[\frac{2\alpha\gamma_s/d}{\Delta g^{ch} + \Delta g^{\sigma}_{max} + g_{el} + W_f}\right] \qquad (13)$$

where all parameters have the same meaning as defined in the previous chapter except for N_v^{o}. However, it is not clear that the same values of parameters can be applied in the strain-induced regime. N_v^{o} in this case is the total number of nucleating defects which will have been created after plastic deformation to the strain e.

If deformation exceeds the elastic limit of a material , nucleation sites will be activated by an applied stress and created by plastic strains, simultaneously. The simplest model of deformation-induced nucleation is to assume that these mechanisms both contribute to the density of nucleation sites, i.e., the effects from both are additive. Then the change in the potency distribution of nucleation sites during deformation will be expressed by a simple equation as :

$$N_v = N_v^{oo} \exp (- \alpha_0 n_0) + N_v^{o} \exp (- \alpha_1 n_1) \qquad (14)$$

where n_o and n_1 are given by

$$n_0 = - \left[\frac{2 \alpha \gamma_s / d}{\Delta g^{ch} + (\Delta g^{\sigma}_{max} / 3) + \Delta g_{el} + W_f} \right] \quad \text{and} \quad n_1 = - \left[\frac{2 \alpha \gamma_s / d}{\Delta g^{ch} + \Delta g^{\sigma}_{max} + g_{el} + W_f} \right] \qquad (15)$$

and N_v's and α's will have different values. It can be inferred from the nature of strain-induced nucleation that the value of N_v° in a function of strain ε.

3-2. Kinetics of Deformation-Induced Transformation

The kinetics of martensitic transformation by the faulting mechanism has been treated by Cohen and Olson[6]. If the original nucleating defects are randomly distributed throughout the volume, the probability p that an austenite particle of volume V_P will contain at least one such defect can be given by :

$$p = 1 - \exp (-N_v \, V_p) \tag{16}$$

where N_v is the number density of nucleation sites per unit volume. If sites occur only on the particle surface, a similar function of surface area will be obtained. For a large number of small particles, the fraction f of particles transformed to martensite will be f=p. Therefore, f is given by :

$$f = 1 - \exp\left[- V_p \left[N_v^{\infty} \exp (- \alpha_0 n_0) + N_v^{o} \exp (-\alpha_1 n_1) \right] \right] \tag{17}$$

Then, the next step is to find the values of N_v's and α's to define the model.

4. Analysis of Transformation Behavior in the Cu-Fe System

Deformation in an aged Cu-Fe alloy which has γ-iron particles in a Cu matrix has been known to induce the martensitic transformation in the iron particles. The transformation behavior of the iron particles has been investigated by several groups[18,19,20,21,22], most extensively by Mori et al.[23,24] They prepared single crystals of a Cu-1.06wt%Fe alloy having different average austenite particle size and measured the fraction of transformed particles with respect to several tensile strains. At present, their results are the most comprehensive available for the study of deformation-induced transformation, especially for strain-induced nucleation kinetics, not only because of its completeness but also due to the relative simplicity of the system compared with steels containing a number of alloying elements. Therefore, their results and some other results will be used to analyze the transformation kinetics in the Cu-Fe system.

4-1. Review of the Data

Mori et al.[25] prepared single crystals of Cu-1.06wt% alloy and produced spherical austenitic iron particles with diameters ranging from 10nm to 160nm by changing the time and temperature of annealing. They carried out tensile tests at several temperatures and measured the fraction f of

particles transformed to martensite after plastic strain. Their results are replotted in Fig.1. It is seen in the figure that the fraction f increases rapidly with the particle size as well as the amount of strain. The fraction also increases as temperature decreases. These trends are in qualitative agreement with the results obtained by Matsuura et al.. The smallest size of the transformed particles decreases as the amount of the strain increases, but it can be inferred that there is a critical size below which martensitic transformation will not occur even when the strain is large. Fig.2 shows the change in the fraction transformed with respect to the amount of true plastic strain in different sizes of particles. The transformation behavior in this figure clearly indicates the characteristic sigmoidal shape and saturation under 100% transformation of strain-induced nucleation.

The transformation behavior of dispersed austenite particles in a Cu matrix was also studied by Matsuura et al.[21] for several Cu-Fe alloys including the same composition as used by Mori[24]. They also provided a set of data on the work hardening behavior during deformation.

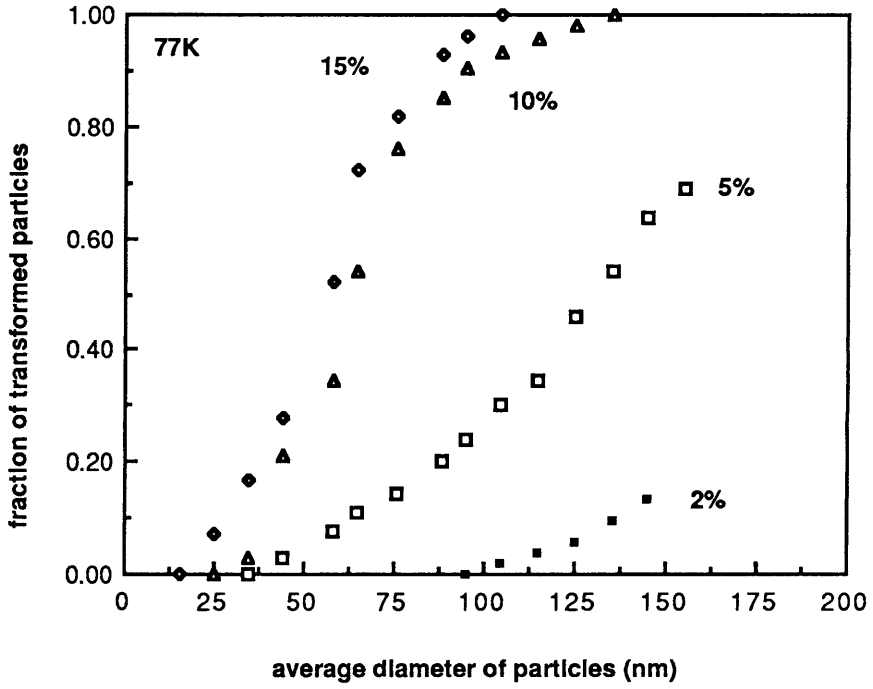

Fig.1-a Change in the fraction of transformed austenitic iron particles in the Cu-Fe alloy single crystal with particle size at 77K for several tensile strains

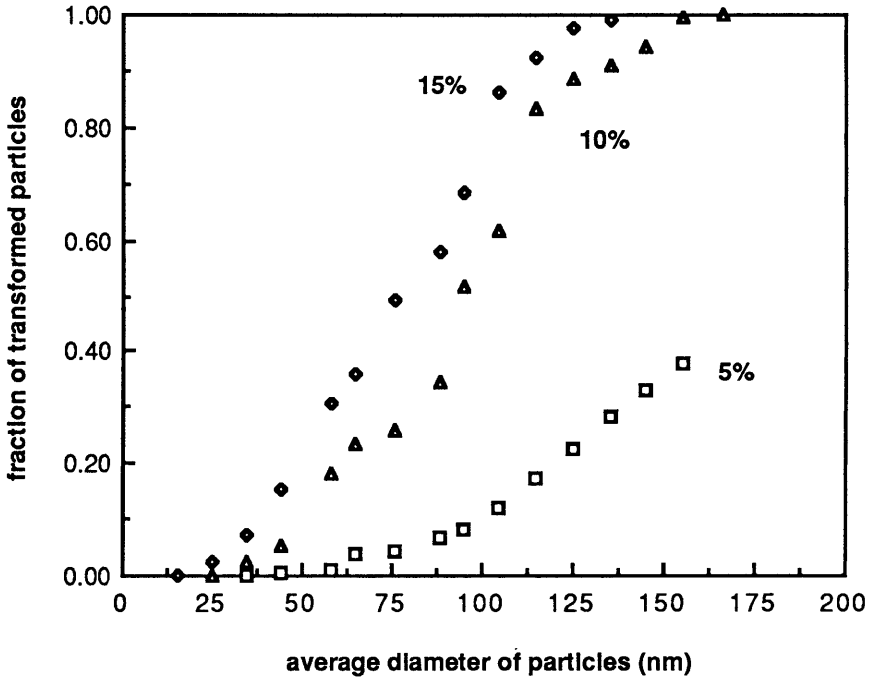

Fig.1-b Change in the fraction of transformed austenitic iron particles in the Cu-Fe alloy single crystal with particle size at 200K for several tensile strains

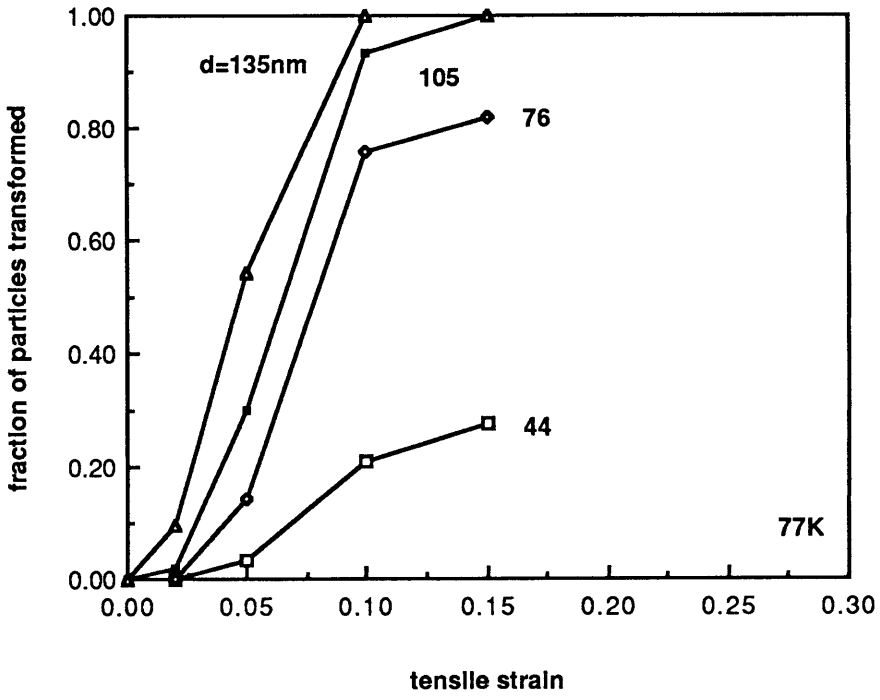

Fig.2-a Change in the fraction of transformed austenitic iron particles in the Cu-Fe alloy single crystal with tensile strain for several particle sizes at 77K

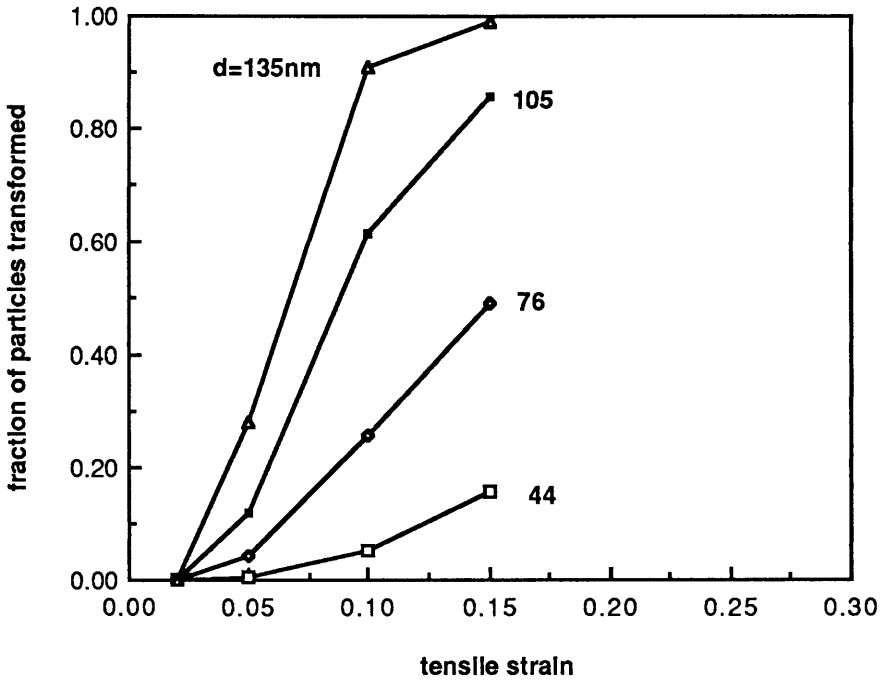

Fig.2-b Change in the fraction of transformed austenitic iron particles in the Cu-Fe alloy single crystal with tensile strain for several particle sizes at 200K

4-2. Estimation of Parameters

First, we will determine the site of the nucleating defect (surface or volume) from Fig.1. Eq.(11) can be modified as :

$$f = 1 - \exp\left[- k N_v (d / 2)^n \right] , \quad \text{and then}$$

$$\log\left[\frac{1}{k N_v} \left[\log (1 / 1\text{-}f) \right] \right] = n \log\left[\frac{d}{2} \right] \qquad (18)$$

where d is the diameter of the austenite particles and k and n are constants. The plot of log(log(1/1-f)) vs log(d/2) distinguishes the volume or surface nucleation depending on the value of n, that is, n=3 means volume nucleation and n=2 implies surface nucleation. Fig.3 shows the above log-log plot for both 77k and 200k test data, in which data points under f=0.1 are omitted because of uncertainty in measurement. The values of n range from 2.7 to 3.3, thus implying volume nucleation. Therefore, n is assumed to be 3 throughout this analysis.

The next step is to estimate the change in N_v with temperature and strain. This is done by fitting the data in Fig.1 using Eq.(11). The results of curve fitting for deformation at 77 and 200K are shown in Fig.4 and the values

of N_v at 77 and 200K from Mori et al., and 300K from Matsuura et al. are tabulated below. It should be noted that Eq.(11) can predict the transformation behavior surprisingly well in spite of its simple form. Fig.5 plots the change in N_v with respect to true plastic strain in a semi-log plot, showing a steep increase in N_v with increasing strain, and the existence of an apparent saturation level.

Table1. Values of N_v

temp.(k)	tensile strain (%)	N_v ($1/m^3$)
77	2	7.407×10^{13}
	5	6.071×10^{14}
	10	4.212×10^{15}
	15	7.454×10^{15}
	116	2.011×10^{17}
200	5	2.461×10^{14}
	10	1.917×10^{15}
	15	3.105×10^{15}
	100	2.011×10^{17}
300	22	3.554×10^{15}
	42	1.676×10^{16}
	64	2.728×10^{17}
	94	5.986×10^{17}

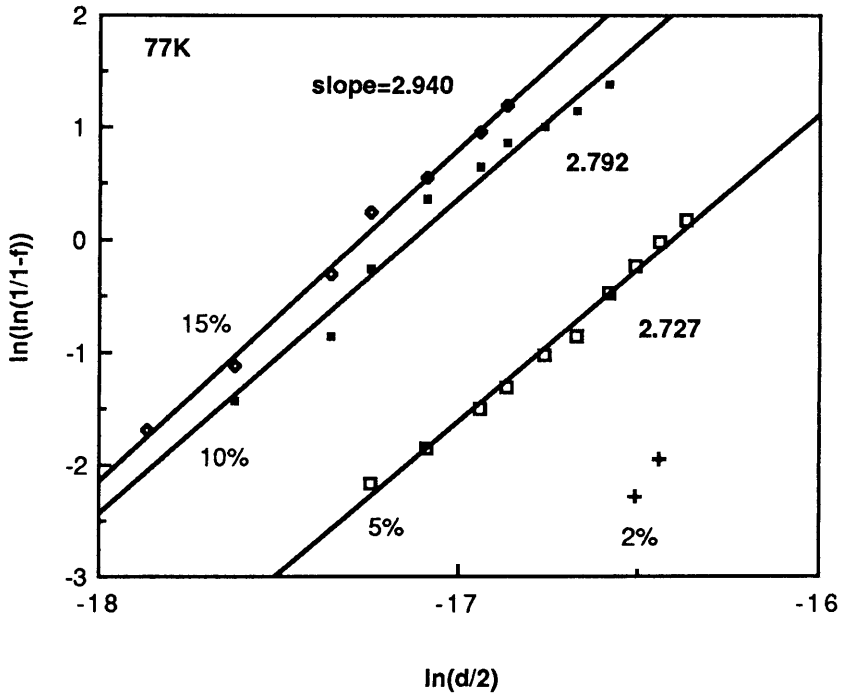

Fig.3-a Determination of the site for nucleation, i.e., volume nucleation or surface nucleation, in austenitic iron particles at 200K

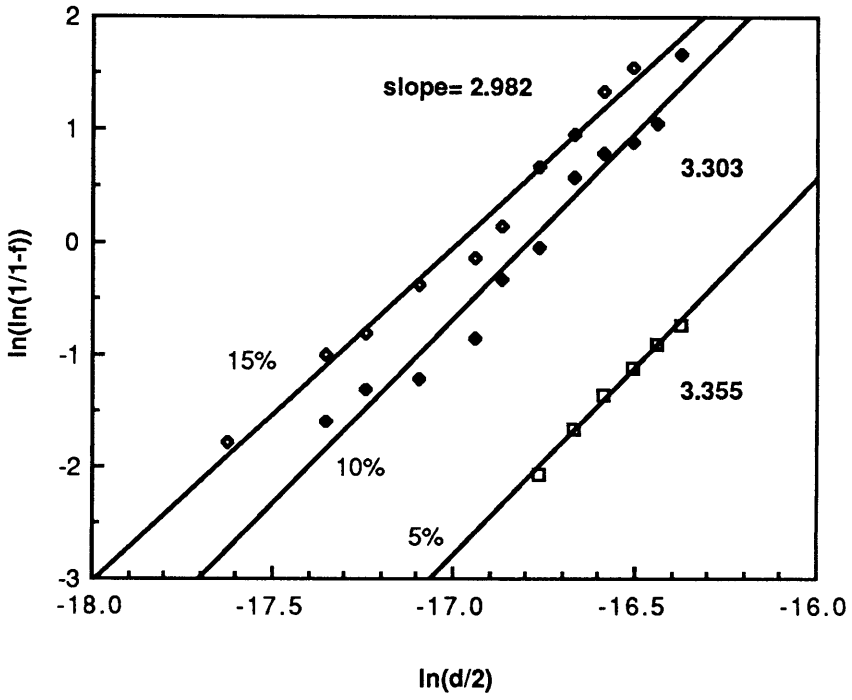

Fig.3-b Determination of the site for nucleation, i.e., volume nucleation or surface nucleation, in austenitic iron particles at 200K

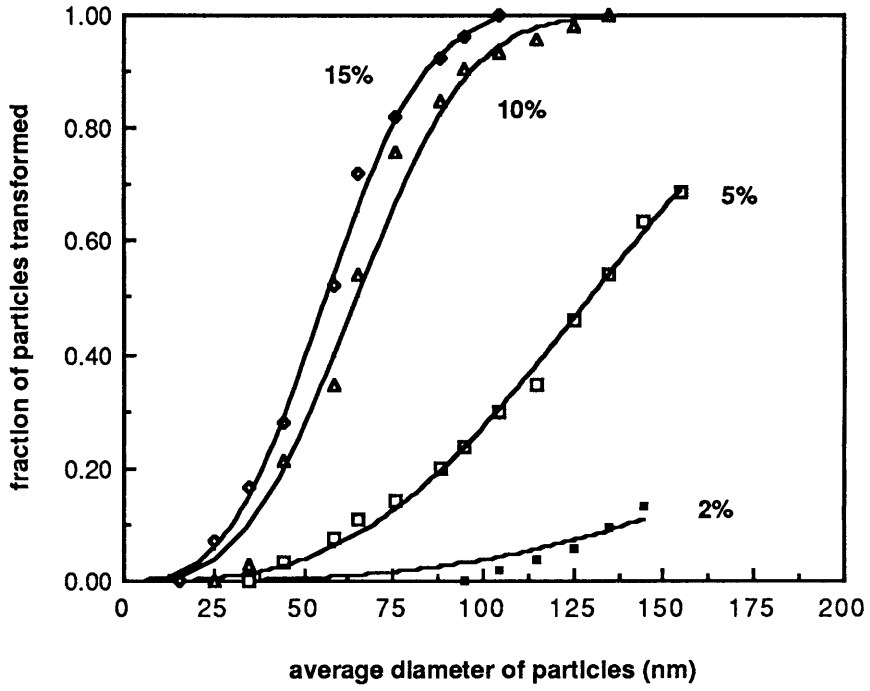

Fig.4-a Best fit of the deformation-induced transformation behavior of austenitic iron particles the Cu-Fe alloy single crystal at 77K by the equation, f=1-exp(-NvVp)

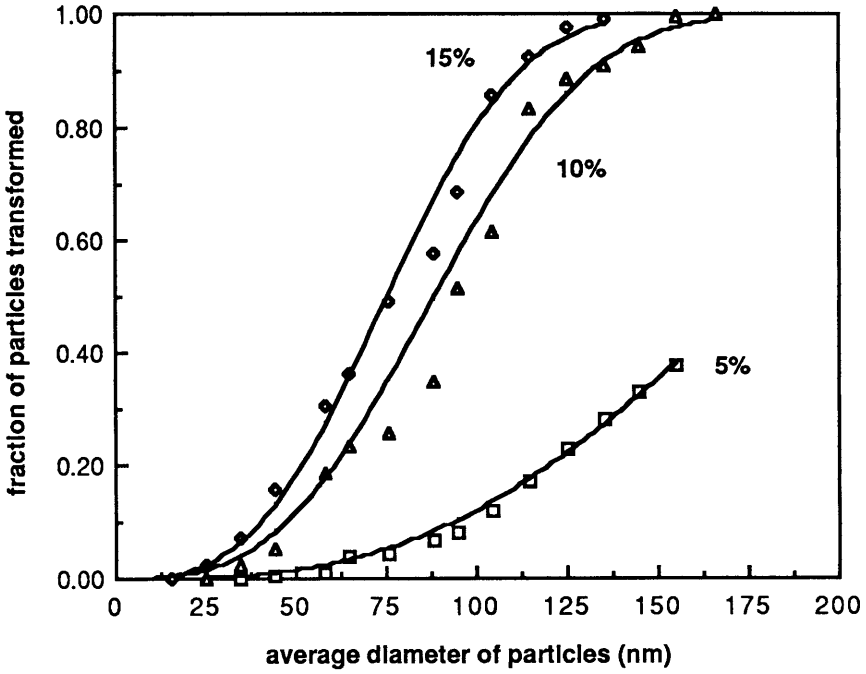

Fig.4-b Best fit of the deformation-induced transformation behavior of austenitic iron particles the Cu-Fe alloy single crystal at 200K by the equation, f=1-exp(-NvVp)

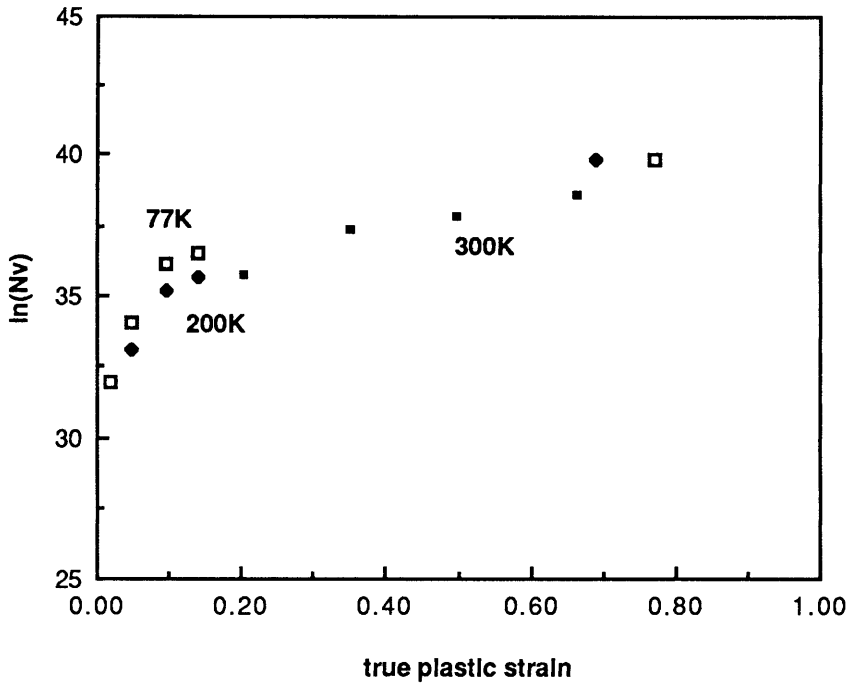

Fig.5 Change in the number density of nucleation sites with true plastic strain for several temperatures

Although the plot in Fig.5 implies a very smooth function for each temperature, the potency distribution should be expressed by Eq.(9) with unique values of α for stress-assisted and strain-induced, respectively, regardless of the temperature. The values of α, $N_v^{\circ\circ}$, and N_v° for different nucleation mechanisms have been determined as follows.

Since the values of Nv tabulated above include contributions from both stress-assisted and strain-induced nucleation, they should be divided into two parts according to Eq.(9). For stress-assisted nucleation in Fe-Ni alloys, Olson and Tsuzaki have obtained the values of $N_v^{\circ\circ}$ and α_0 as $2x10^{17}$ ($1/m^3$) and 0.84, respectively. If the same defect-potency distribution applies for stress-assisted nucleation in Fe-alloys, the same value of α_0 should be used in the present case, though $N_v^{\circ\circ}$ might have a different magnitude due to the difference in alloy system and history. The value of $N_v^{\circ\circ}$, the total number density of defects of all potencies without strain, is obtained from the data of Matsuura et al[21].. They used the same Cu-Fe system with a wider range of Fe content and measured the change in the fraction of austenite particles transformed into martensite under deformation. One of their results on a Cu-1.5wt%Fe alloy shows that martensitic transformation takes place during cooling, though the amount is very small and scattered. This is the only result available

for the Cu-Fe system to estimate $N_v^{\circ\circ}$. From this, $N_v^{\circ\circ}$ is obtained as 3.5×10^{14} ($1/m^3$). Therefore, the stress-assisted part of Eq(9) becomes :

$$N_v = 3.5 \times 10^{14} \exp (- 0.84 n_0) + N_v^{o} \exp (- \alpha_1 n_1) \quad (1 / m^3) \tag{19}$$

The change in the number density of sites due to the strain-induced nucleation thus can be obtained by :

$$N_v \text{ (strain-induced)} = N_v^{o} \exp (- \alpha_1 n_1) = N_v - 3.5 \times 10^{14} \exp (- 0.84 n_0) \quad (1 / m^3) \tag{20}$$

Fig.6 shows the change in N_v(strain-induced) with respect to true plastic strain in semi-log form. It is to be noted that the rate of increase in nucleation sites is very large during initial small plastic strains and then decreases, and the number of sites seems to saturate at large plastic strains. In order to obtain the values of N_v° and α_1, values of n_1, i.e., number of atomic planes in a nucleating defect given by Eq.(10), are required. In Eq.(10), γ_s and $g_{el}+w_f$ are assumed to be the same value as obtained by Olson and Tsuzaki, i.e., 0.15 J/m^2 and 6.1×10^7 J/m^3, respectively. d is taken to be 2.11×10^{-10} m, the close-packed interplanar spacing of pure FCC iron, since γ-particles in a Cu-matrix are considered to

be pure. Δg^{ch} for pure iron is given by the following equations : for temperature from 1 to 300K,

$$\Delta g^{ch} = - 5451.752 - 7.4475 \times 10^{-3} T^2 + 1.2 \times 10^{-4} T^3 - 2.05434 \times 10^{-7} T^4 \quad (J / mole) \tag{21}$$

for temperature from 300 to 1100K,

$$\Delta g^{ch} = - 6108.64 + 3.4618 T + 7.472 \times 10^{-3} T^2 - 5.124 \times 10^{-6} T^3 \quad (J / mole) \tag{22}$$

Estimation of Δg^{σ}_{max} requires tensile stress-strain relations during plastic straining at each deformation temperature. Mori et al. do not give stress-strain relations for their materials, while Matsuura et al. show relations for 3 different temperatures, 77, 200, and 300K and for two different diameter of γ-particle, 30 and 106nm, though those relations are expressed in the form of shear stress-shear strain curves. Since the Fe contents of the Cu-Fe alloys used by Matsuura et al. are almost the same as that of Mori's specimens and diameter of γ-particle falls within the range of Mori's experiments, it can be assumed that the specimens of Mori's experiment have the same stress-strain relations as those of Matsuura's specimens. Therefore, the tensile stress-strain relationship is obtained by transforming shear

stress and shear strain into tensile stress and strain, using the relation given by Christian et al[25].. The results are shown in Fig.7 and Fig.8 for two alloys containing small and large γ-particles. From these figures, it is seen that the differences in stress level and work hardening behavior are consistent with those observed in the shear stress-strain curves. The most important differences among them are the lower yield stress of alloys having larger diameter particles, implying that there is an effect of transformation induced plasticity on work hardening behavior of these alloys. For the purpose of estimation of Δg^{σ}_{max}, stress-strain curves for alloys containing small γ-particles in Fig.7 are used. The values of the transformation shear strain parallel to the habit plane, γ_0, and the dilatational strain normal to the habit plane, ε_0, are assumed to be the same as those used by Olson-Tsuzaki, 0.2 and 0.04 respectively.

The number of atomic planes in a nucleating defect obtained using the above values ranges from 1.9 to 2.4. Such small numbers of n for transformation in small particles has also been observed in ceramic systems[17].

Fig.9 shows a plot of the change in the number density of nucleation sites with n for estimating α_1 for strain-induced nucleation. Using upper-bound values of log[Nv-Nv(stress)],

α_1 has been determined as 3.88. Fig.10, which shows a set of lines having a slope of -3.88 on the same plot as Fig.9, gives a fairly good prediction of Nv(strain-induced). From this α_1 and values of n_1 obtained before, Nv° for strain-induced nucleation has been determined as represented in Table 2.

Fig 11 is a plot of natural log of N_v° with respect to true plastic strain and indicates a very steep increase in N_v° toward a saturation level. It should be noted in this plot that the strain dependence of N_v° can be expressed by only one equation in spite of the difference in temperature. Taking into account the existence of a certain saturation level, N_v° can be a function of the form :

$$N_v^o(\varepsilon) = N\left[1 - \exp(-k\varepsilon^n)\right] \qquad (23)$$

where N, k, and n are constants and ε is the true plastic strain. A best fit of the points on Fig.11 by this equation is shown in Fig.12 with 5% of error on each point, resulting in $N=4.79\times10^{20}$ $(1/m^3)$, k=46.0, and n=3.45, and the final form becomes :

$$N_v^o(\varepsilon) = 4.79 \times 10^{20}\left[1 - \exp(-46.0\,\varepsilon^{3.45})\right] \ (1/m^3) \qquad (24)$$

Table. 2 N_v-N_v(stress) and N_v°

Temp. (K)	Plastic Strain	N_v-N_v(stress)	N_v° ($1/m^3$)
77	0.02	9.198×10^{12}	2.176×10^{16}
	0.049	5.422×10^{14}	1.233×10^{18}
	0.095	4.813×10^{15}	1.086×10^{19}
	0.14	7.454×10^{15}	1.654×10^{19}
	0.772	2.011×10^{17}	3.313×10^{20}
200	0.049	1.884×10^{14}	7.317×10^{17}
	0.095	1.859×10^{15}	7.136×10^{18}
	0.14	3.047×10^{15}	1.161×10^{19}
	0.691	2.011×10^{17}	6.141×10^{20}
300	0.202	3.509×10^{15}	4.231×10^{19}
	0.349	1.672×10^{16}	1.046×10^{20}
	0.497	2.723×10^{16}	2.923×10^{20}
	0.665	5.981×10^{16}	6.151×10^{20}

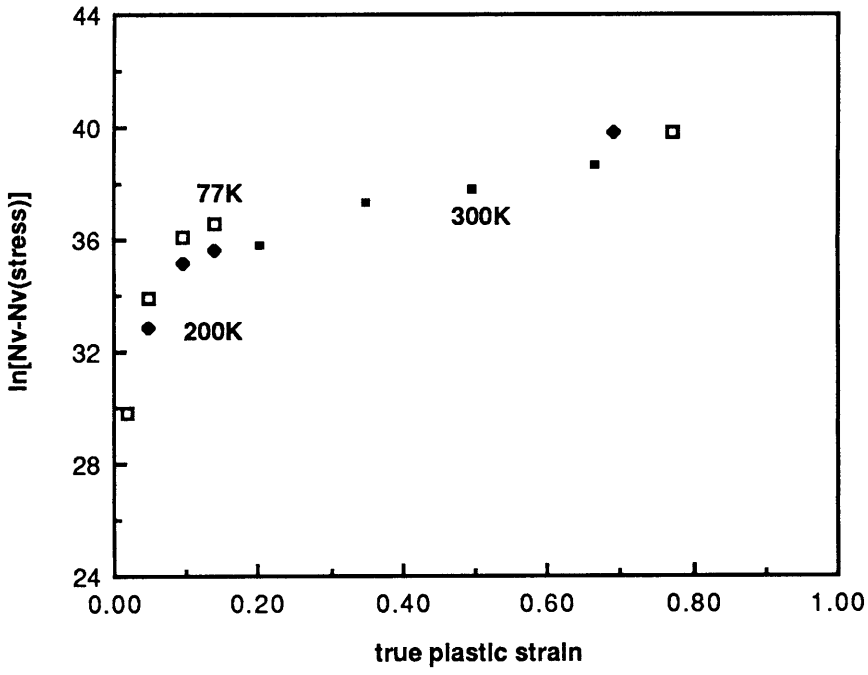

Fig.6 Change in the number density of nucleation sites created by plastic strain through strain-induced nucleation

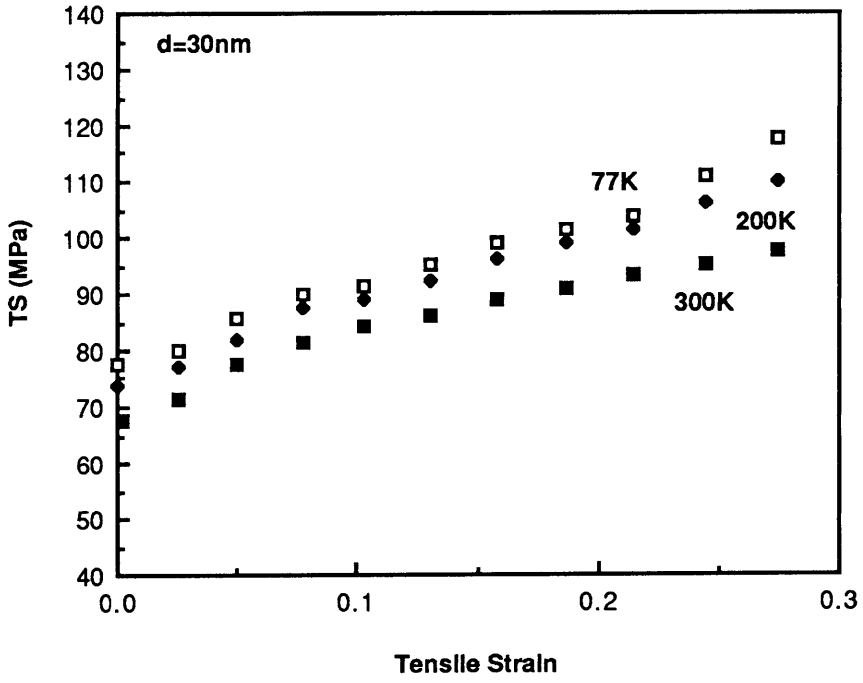

Fig.7 Tensile stress-strain relations of the Cu-Fe alloy single crystal containing austenitic iron particles having the average diameter of 30nm for several temperatures

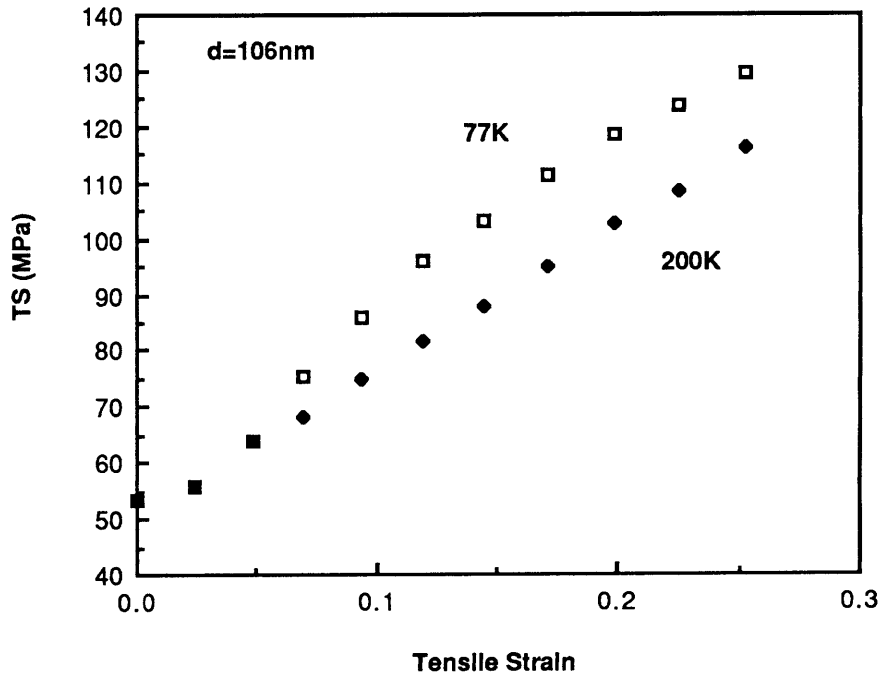

Fig.8 Tensile stress-strain relations of the Cu-Fe alloy single crystal containing austenitic iron particles having the average diameter of 106nm for several temperatures

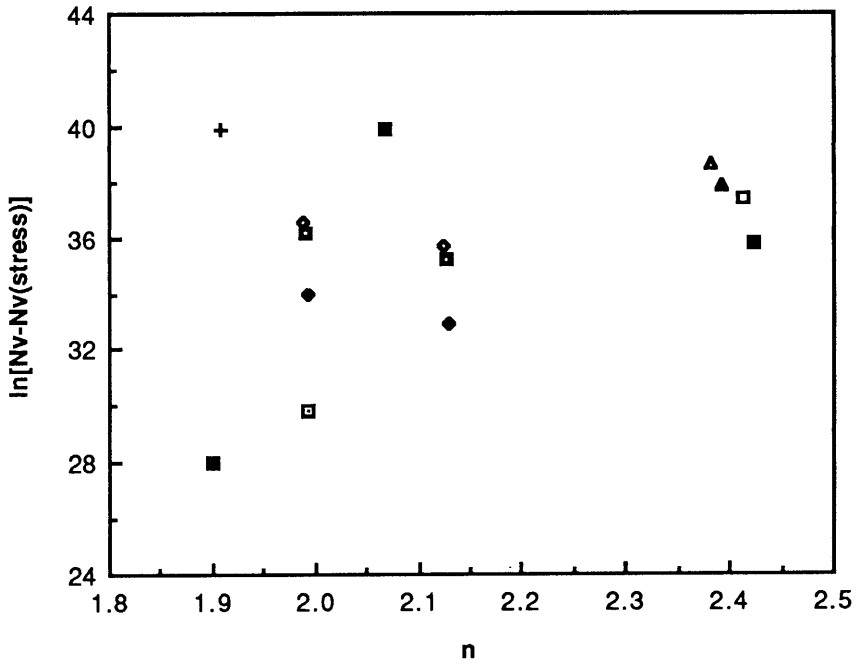

Fig.9 Change in the number density of nucleation sites with the number of atomic planes in a defect for the strain-induced nucleation

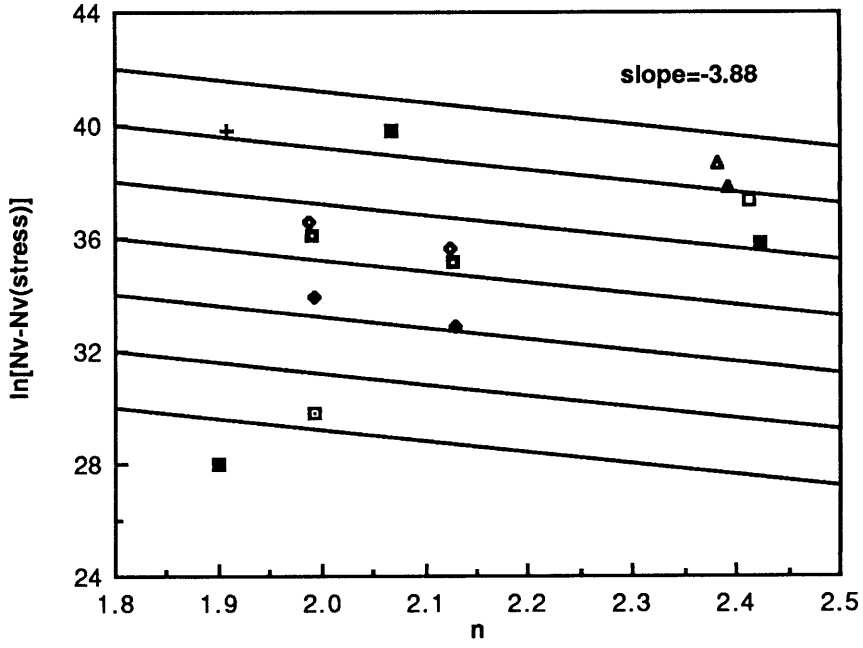

Fig.10 Determination of the distribution shape factor for strain-induced nucleation, an absolute value of the slope is the distribution shape factor

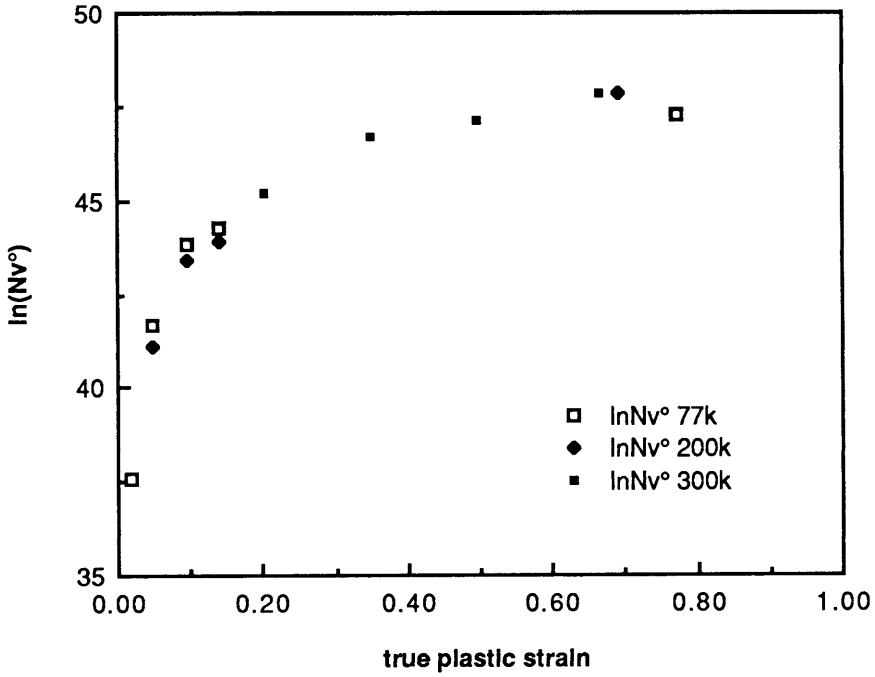

Fig.11 Change in the total number of nucleation sites of all potencies with true plastic strain for strain-induced nucleation

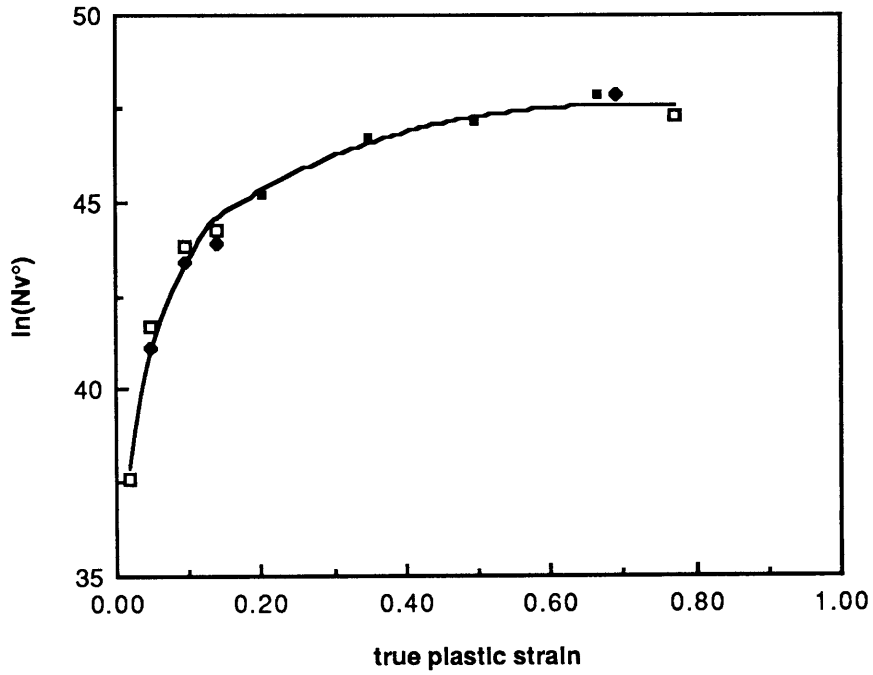

Fig.12 Prediction of the change in the total number of nucleation sites of all potencies with true plastic strain for strain-induced nucleation

The potency distribution when both stress-assisted and strain-induced nucleation are operating is thus given by :

$$N_v = 3.52 \times 10^{14} \exp(-0.84\, n_0) + 4.79 \times 10^{20} \left[1 - \exp(-46.0\, \varepsilon^{3.45})\right] \exp(-3.88\, n_1) \quad (1/m^3) \tag{25}$$

Fig.13 compares the experimentally obtained values of N_v for three different temperatures with those predicted from the above equation and shows that the potency distribution can be predicted fairly well by the model developed here.

4-3. Prediction of Transformation Behavior

The transformation behavior of austenitic particles in a Cu-matrix can then be predicted combining the above potency distribution and Eq.(11). Fig.14 shows the relation between fraction of transformed particles and diameter of particle at 77, 200, and 300K. Fig.15 shows the transformation behavior of γ-particles in terms of true plastic strain. In both predictions, the model has a tendency to give more transformation as the plastic strain increases, though it provides good agreement in some cases. This tendency is thought to be the result of the original scatter in N_v's and uncertainties involved in the determination of N_v°°.

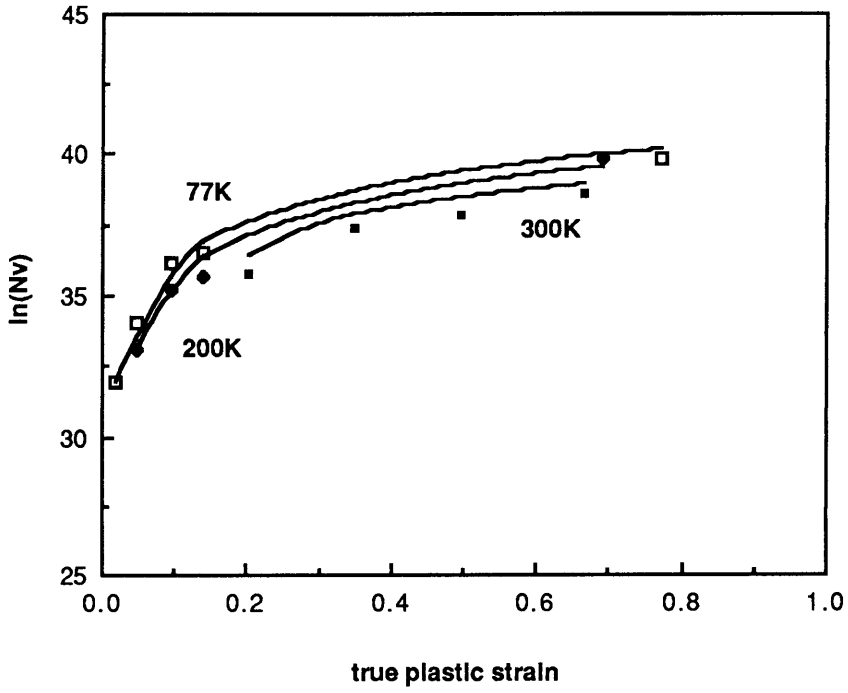

Fig.13 Prediction of the variation of the number density of nucleation sites with strain from the kinetic model

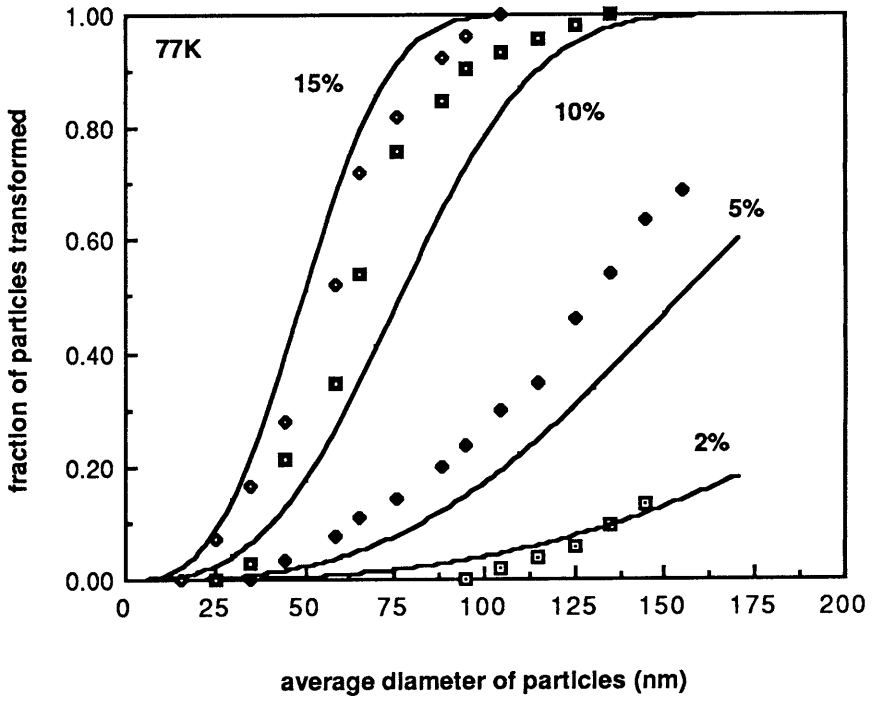

Fig.14-a Prediction of the deformation-induced transformation behavior of austenitic iron particles in the Cu-Fe alloy single crystal with particle diameter for several tensile strains at 77K

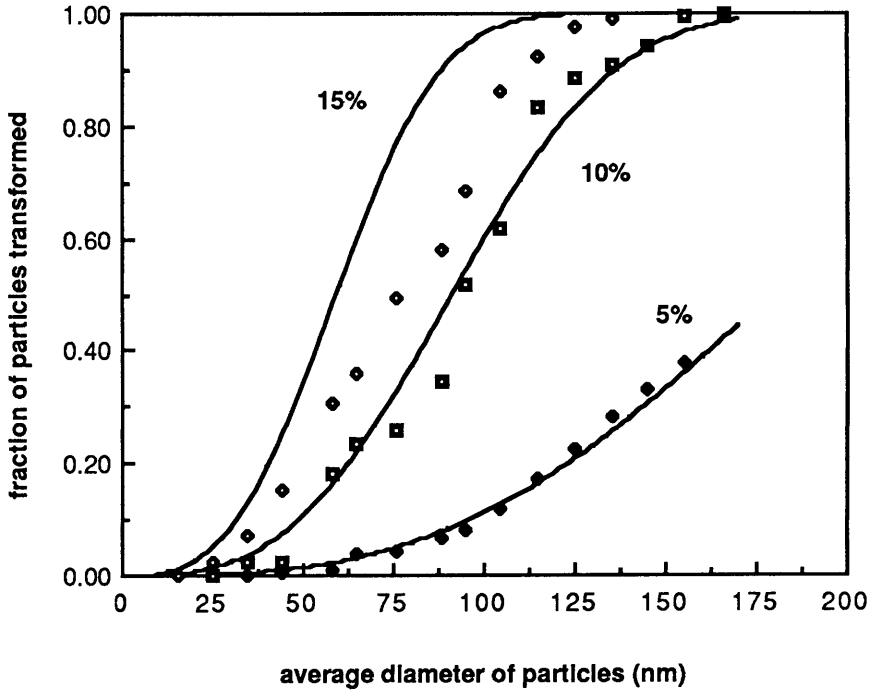

Fig.14-b Prediction of the deformation-induced transformation behavior of austenitic iron particles in the Cu-Fe alloy single crystal with particle diameter for several tensile strains at 200K

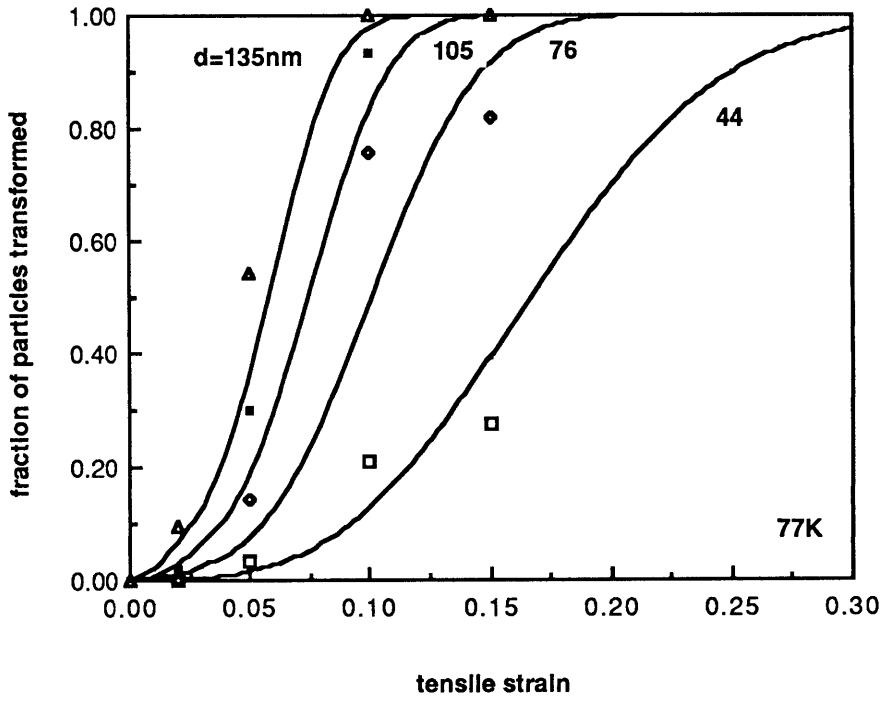

Fig.15-a Prediction of the change in the fraction of deformation-induced transformation behavior of austenitic iron particles in the Cu-Fe alloy single crystal with strain for several particle sizes at 77K

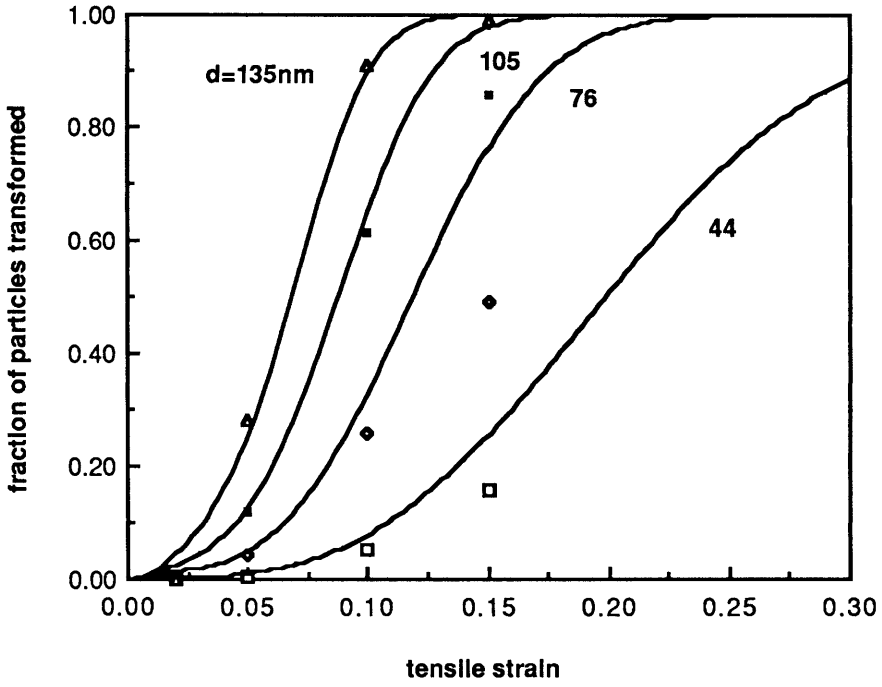

Fig.15-b Prediction of the change in the fraction of deformation-induced transformation behavior of austenitic iron particles in the Cu-Fe alloy single crystal with strain for several particle sizes at 200K

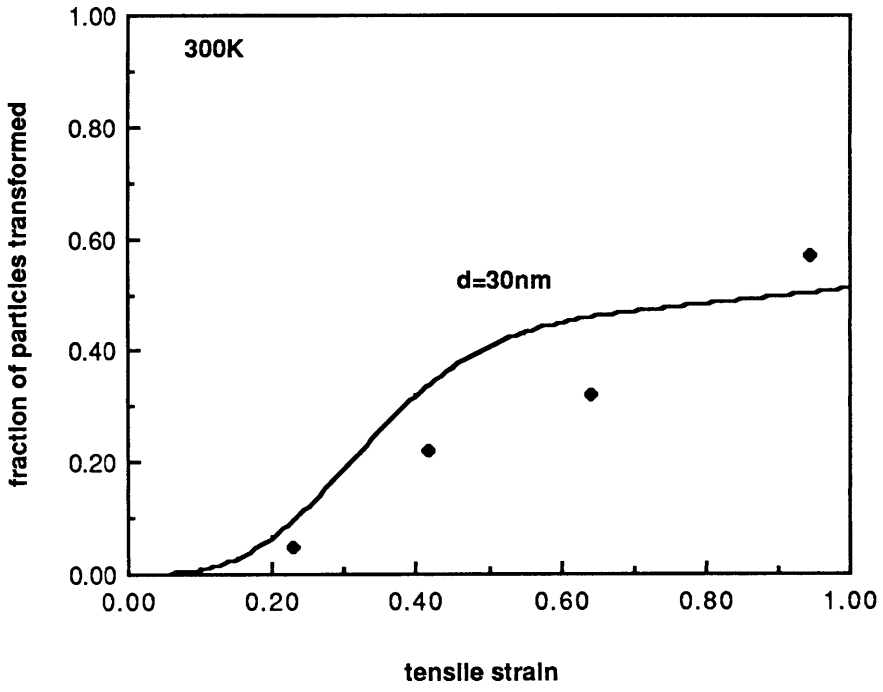

Fig.15-c Prediction of the change in the fraction of deformation-induced transformation behavior of austenitic iron particles in the Cu-Fe alloy single crystal with strain at 300K

5. Application of the Model to a "Dual-Phase" Steel

"Dual phase" steels generally consist of about 80 vol.% ferrite and the balance of a mixture of martensite and retained austenite, and show a low yield strength, a high initial strain-hardening rate, and a high uniform ductility compared with steels having the same compositions but different microstructures. Recently, retained austenite has received increased attention as a source of dispersed phase transformation plasticity.

Recent study by Sachdev[26] has shown clearly the influence of retained austenite on the deformation behavior of the dual phase steels. He has analyzed the transformation behavior and its effects quantitatively at several temperatures, thus providing a good place for examining our simple model of deformation-induced transformation.

5-1. Review of the Data

Sachdev made samples from a production coil of a vanadium containing dual phase steel whose chemical composition, production history, and mechanical properties are listed in Table 3. Samples were tensile tested at a nominal strain rate of 10^{-3} s^{-1} at temperatures between 220 and 460K.

Retained austenite contents were determined by X-ray diffraction after straining at test temperatures from 295 to 400K. The change in the fraction of retained austenite transformed into martensite and the volume fraction of martensite in the steel are shown in Figs. 16 and 17, respectively.

Table 3. Properties of the dual phase steel

Chemical composition (wt.%)	
C	0.12
N	0.007
Mn	1.44
Si	0.50
V	0.061
Annealing condition	
4 min. at 788 °C, then forced air cooling	
Mechanical properties	
Yield Strength	367 MPa
Ultimate Tensile Strength	639 MPa
Uniform elongation	23 %
Total elongation	32 %

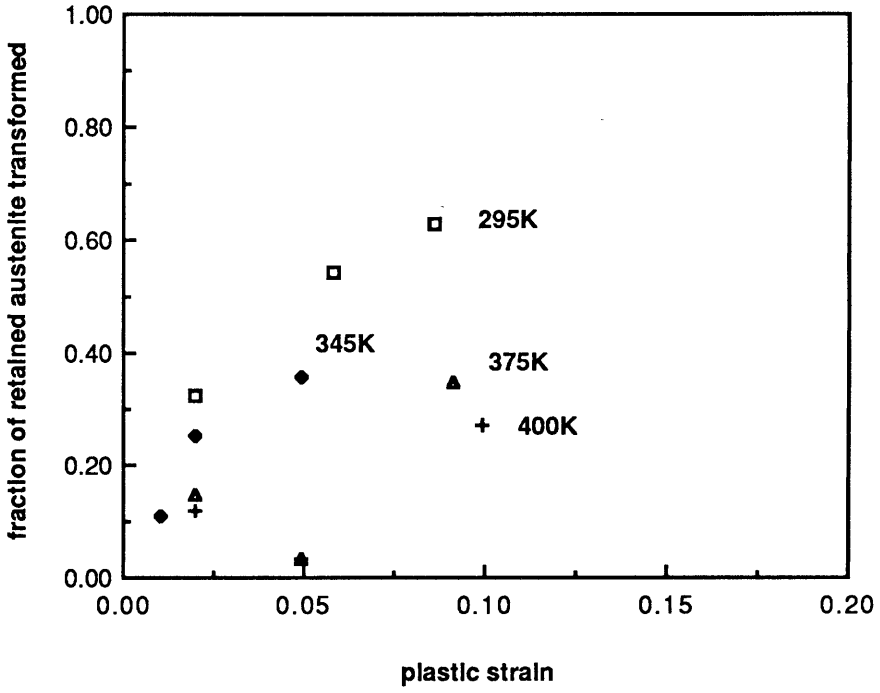

Fig.16 Variation of the fraction of transformed retained austenite in the dual phase steel with true plastic strain

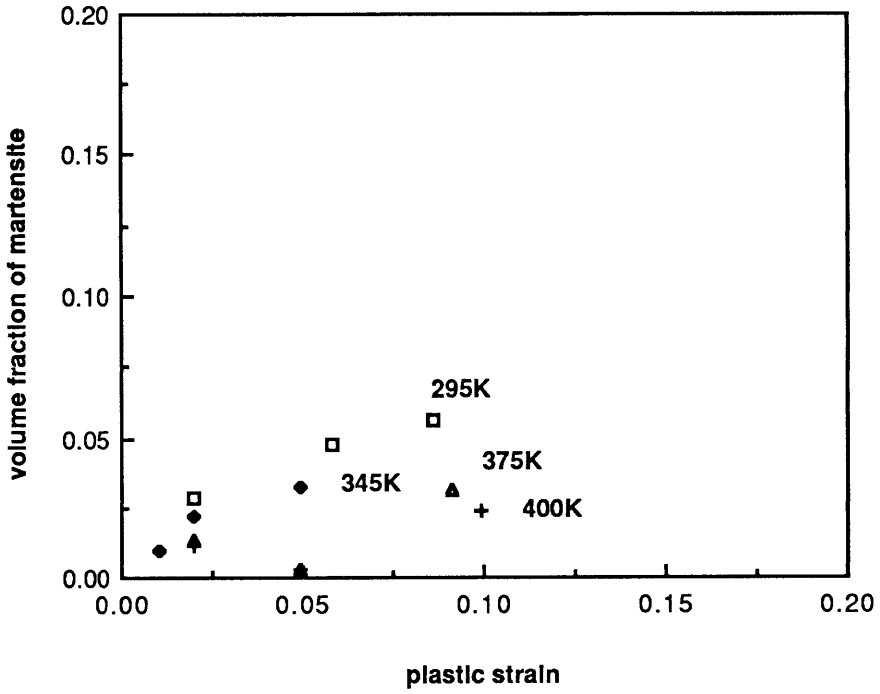

Fig.17 Variation of the volume fraction of martensite transformed from the retained austenite in the dual phase steel with true plastic strain

The fraction of retained austenite transformed increases with increasing plastic strain but shows a somewhat different behavior from the Cu-Fe alloys, partly due to the difference in stability of austenite and partly due to a greater contribution from stress-assisted nucleation.

In order to apply the model, the role of these factors must be estimated quantitatively.

5-2. Estimation of Parameters

5-2-1. Estimation of average volume of retained austenite and stress-strain relations

In order to calculate the constants in Eq.(9) to express the potency distribution in the retained austenite, the following quantities are to be estimated; that is, the average particle volume for estimation of N_V and the stress-strain relations for estimation of the mechanical driving force.

The average volume of retained austenite is necessary to obtain the experimental values of site density and to predict the transformation behavior. This has been estimated from transmission electron micrograph of the same material as that of Sachdev's experiment. The retained austenite observed[27] has a lath-like shape and a very thin thickness compared with its length and width, which is consistent with

the observation of Rigsbee et al.[4] and Furukawa et al.[3]. Assuming the shape of the observed austenite as an oblate spheroid, the average volume has been estimated as $V_p=1.76x10^{-13}$ m^3.

Tensile stress-strain relations have been given by Sachdev for the same materials used to measure the transformation behavior. Within the small plastic strain region in which the retained austenite transformed, the tensile stress has been assumed to have a linear relation with tensile strain. These equations are given as :

$$TS\,(MPa) = 36.7\,e + 353.5 \quad (295K), \qquad TS\,(MPa) = 49.6\,e + 340.3 \quad (345K)$$
$$TS\,(MPa) = 55.6\,e + 332.5 \quad (375K), \qquad TS\,(MPa) = 58.4\,e + 320.3 \quad (400K)$$

(26)

5-2-2. Estimation of effects of alloying elements on stability of retained austenite

Most alloying elements except for Co and Al stabilize austenite. Thus, chemical composition of the retained austenite is very important in order to estimate the contribution of stabilizing effects to the overall driving force of martensitic transformation.

5-2-2-1. Chemical effects

Austenite stabilizing elements, such as Ni, Mn, C, and Cu, lower the T_0 temperature, where free energies of austenite

and martensite are equal, thus chemically stabilize austenite. In other words, C and Mn increase the energy barrier to start martensitic transformation. C and Mn have higher solubility in austenite than in ferrite and are considered to be enriched in the austenite phase even after a short time of intercritical annealing because austenite can nucleate and grow on cementite particles which have high Mn and C contents. Therefore,.it is quite difficult to estimate the chemical composition of retained austenite because austenite is not in equilibrium with the surrounding ferrite during a short time of intercritical annealing and following relatively fast cooling to room temperature. However, some data have been obtained from equilibrium thermodynamics and scanning transmission electron microscope analysis. The Mn content has been obtained by STEM analysis as 2 wt%[28].

The paraequilibrium phase diagram obtained by thermodynamic analysis[28,29] shows that the equilibrium carbon content in the retained austenite is approximately 0.5 wt% provided that there is no redistribution of Mn between ferrite and austenite during the intercritical annealing. The true equilibrium phase diagram with Mn redistribution[29,30] indicates that the carbon content is about 0.52 wt% when the Mn content is about 2 wt%. Therefore, after taking into

account the non-equilibrium state of annealing, the carbon content can be assumed to be 0.5 wt% as an upper limit.

The method for estimating the Si and V contents in the retained austenite is not available at the present time. Hence, the same amount of Si and V as in the original alloy is assumed to exist in the retained austenite.
The chemical composition thus defined then permits an estimate of the chemical free energy difference between austenite and martensite from the data bank of Thermocalc and the result is

$$\Delta g^{ch} = -5290 + 6.543\,T \quad (J / mole) \tag{27}$$

5-2-2-2. Mechanical effects

Alloying elements such as C, Mn, Cr, and Ni which have a significant solid solution hardening effect on the mechanical properties of austenite will increase the resistance against shear deformation, thus retarding the overall transformation kinetics. This so-called mechanical stabilization will increase the amount of the frictional work of interfacial motion, W_f. In the present alloy, both carbon and manganese segregate in the austenite phase and produce solid-solution hardening. Therefore, contributions from these elements should be included in the calculation of the potency

distribution. Si also has a strong solution-hardening effect. However, data available are so small that the effect is neglected in the present study.

The composition dependence of W_f can be obtained from available data for the composition dependence of the transformation critical driving force in alloys.
Using the regular solution approximation, the molar free energies of the bcc phases in binary Fe-X and ternary Fe-X-Y alloys are given by :

$$g^{\alpha} = x^{\alpha}_{Fe}\, g^{\alpha}_{Fe} + x^{\alpha}_{X}\, g^{\alpha}_{X} + x^{\alpha}_{Fe}\, x^{\alpha}_{X}\, \Omega^{\alpha}_{FeX} + R\,T\,(\, x^{\alpha}_{Fe} \ln x^{\alpha}_{Fe} + x^{\alpha}_{X} \ln x^{\alpha}_{X}\,)$$

$$g^{\alpha} = x^{\alpha}_{Fe}\, g^{\alpha}_{Fe} + x^{\alpha}_{X}\, g^{\alpha}_{X} + x^{\alpha}_{Y}\, g^{\alpha}_{Y} + x^{\alpha}_{Fe}\, x^{\alpha}_{X}\, \Omega^{\alpha}_{FeX} + x^{\alpha}_{Fe}\, x^{\alpha}_{Y}\, \Omega^{\alpha}_{FeY} + x^{\alpha}_{X}\, x^{\alpha}_{Y}\, W^{\alpha}_{XY} + R\,T\,(\, x^{\alpha}_{Fe} \ln x^{\alpha}_{Fe} + x^{\alpha}_{X} \ln x^{\alpha}_{X} + x^{\alpha}_{Y} \ln x^{\alpha}_{Y}\,) \qquad (28)$$

where x^{α}_{i} is a mole fraction of i in the bcc phase, g^{α}_{i} is the free energy of pure bcc phase of i, W^{α}_{XY} is an interaction parameter between X and Y in the bcc phase which is generally negligible, and Ω^{α}_{FeX} is an interaction parameter between Fe and the alloying element X. The same equations with superscript γ express free energies of the fcc phase in the binary and ternary systems. Then the free energy difference between two phases is given by :

$$\Delta g^{\gamma\to\alpha} = x_{Fe}\,\Delta g^{\gamma\to\alpha}_{Fe} + x_X\,\Delta g^{\gamma\to\alpha}_X + x_{Fe}\,x_X\,\Delta\Omega^{\gamma\to\alpha}_{FeX}$$

$$\Delta g^{\gamma\to\alpha} = x_{Fe}\,\Delta g^{\gamma\to\alpha}_{Fe} + x_X\,\Delta g^{\gamma\to\alpha}_X + x_Y\,\Delta g^{\gamma\to\alpha}_Y + x_{Fe}\,x_X\,\Delta\Omega^{\gamma\to\alpha}_{FeX} + x_{Fe}\,x_Y\,\Delta\Omega^{\gamma\to\alpha}_{FeY}$$

(29)

Ishida and Nishizawa[30] measured the stability of austenite in Fe-Ni-X ternary systems and determined interaction parameters and Ms temperatures, using Kaufman's data[31]. Based on their results for Ms temperatures and Kaufman's latest thermodynamic data[32], the effect of manganese can be obtained as a difference in the values of $\Delta g^{\gamma\to\alpha}$ at $X_{Mn}=0$ at $X_{Mn}=X_{Mn}$ in austenite. The terms of the above equation for Fe-Ni-Mn alloys are given by :

$$\Delta g^{\gamma\to\alpha}_{Fe} = -\,(\,6108.64 - 3.4618\,T - 7.472\times10^{-3}\,T^2 + 5.1254\times10^{-6}\,T^3\,)\quad(\,J/mole\,)$$

$$\Delta g^{\gamma\to\alpha}_{Ni} = -\,(\,-3932.96 - 4.1086\times10^{-3}\,T^2 + 4.8534\times10^{-6}\,T^3 - 1.410\times10^{-9}\,T^4\,)$$

$$\Delta g^{\gamma\to\alpha}_{Mn} = -\,(\,1087.84 + 4.9371\times10^{-3}\,T^2 - 3.1966\times10^{-6}\,T^3\,)$$

$$\Delta\Omega^{\gamma\to\alpha}_{FeNi} = -\,(\,-5648.4 + 6.1923\times10^{-4}\,T^2 + 8.4517\times10^{-7}\,T^3\,)$$

$$\Delta\Omega^{\gamma\to\alpha}_{FeMn} = -\,(\,-24894.8 + 2.5815\times10^{-3}\,T^2\,)$$

(30)

and the results for the driving force at Ms are shown in Fig.18. According to Labusch[33] who treated solid-solution hardening statistically, the critical shear stress to move a

dislocation through a random array of obstacles in the glide plane is proportional to the two-thirds power of the concentration of alloying element. Therefore, as a rough approximation of the effect of Mn on W_f, ΔW_f can be expressed in terms of the two-thirds power of Mn content :

$$\Delta W_{f(Mn)} = 1.893 \times 10^3 X_{Mn}^{2/3} \quad (J / mole) \tag{31}$$

For the effect of carbon, the change in Ms temperature with respect to C content, the free-energy change of pure C and the interaction parameter are required for estimation. Ms data are given by Howard[34] in a graphical form. Thermodynamic data are given by Taylor[35] based on Kaufman et al.[36] and Saunders et al.[37] as follows :

$$\begin{aligned}\Delta g^{\gamma\rightarrow\alpha} = {} & (1 - x_C)(-6108.64 + 3.4618\,T + 7.472 \times 10^{-3}\,T^2 - 5.1254 \times 10^{-6}\,T^3) \\ & + 8368\,x_C \\ & + x_C(1 - x_C)(59412 - 34.894\,T + 60668\,x_C - 8.745\,x_C\,T) \\ & + (-106670 - 0.1393\,T^2)(x_C(0.4 - x_C)/0.16)^2\end{aligned} \tag{32}$$

The results for $\Delta g(Ms)$ are plotted in Fig.19, and ΔW_f can be expressed as :

$$\Delta W_{f(C)} = 1.310 \times 10^{4} X_C^{2/3} \quad (J / mole) \tag{33}$$

Using these equations, the contribution from manganese and carbon have been estimated to be about 1200 J/mole, with X_{Mn}=0.0204 and X_C=0.023.

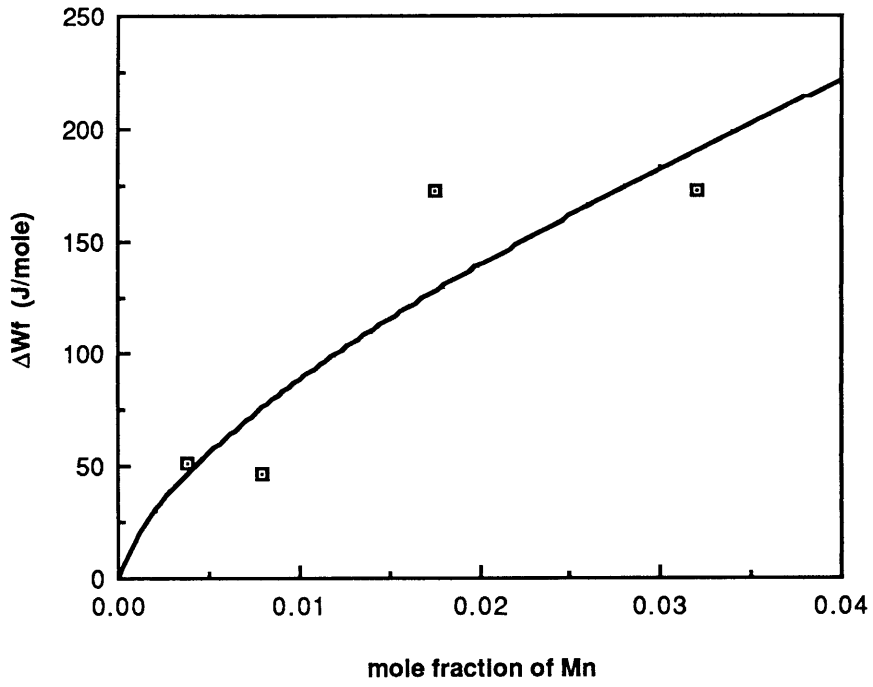

Fig.18 Composition dependence of the frictional work of interfacial motion (Fe-Mn-Ni alloy)

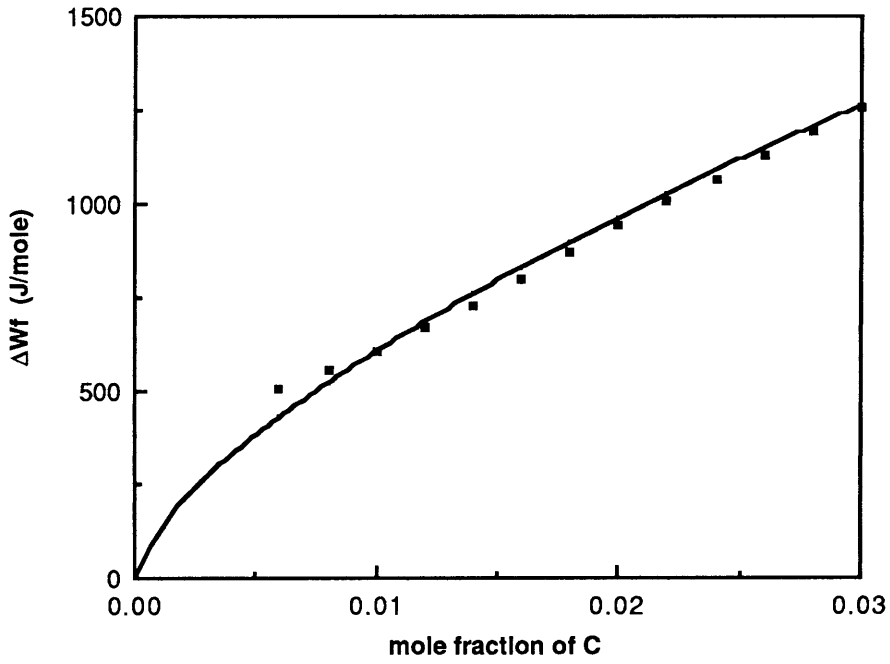

Fig.19 Composition dependence of the frictional work of interfacial motion (Fe-C alloy)

5-2-3. Contribution of stress-assisted nucleation

As seen from Fig.16, the transformation of retained austenite is fairly fast in a small strain region compared to the behavior in the Cu-Fe system. It is also to be noted that the initial increase in f seems not to be sigmoidal but rather resembles to a power-law curve. In other words, the slope is very steep initially and decrease with strain. These facts imply some contribution from stress-assisted transformation at the very beginning.

Two effects are expected from stress-assisted transformation. One is the transformational strain. The strain measured from a tensile test includes the transformational strain produced by the martensitic transformation itself and the slip strain generated by the applied stress. If this transformational strain is large, then it will affect the plot of f vs. strain in such a way that the plot shifts to the smaller strains and the potency distribution due to strain-induced nucleation should be estimated by only using the slip strain.

The other effect is that stress-assisted transformation will generate a certain amount of martensite during elastic deformation so that f is not zero at zero plastic strain.

Hence, it might be more reasonable to regard the f in Fig.16 to start from a nonzero value at zero plastic strain.

Transformational strain can be estimated from the observation of Olson and Azrin[38] that the volume fraction of martensite will initially have a linear relationship with transformational strain below the M_s^{σ} temperature, i.e.,

$$f_v^{\alpha'} = k\,\varepsilon_{transformation} \tag{34}$$

where k is a constant. They have obtained the value of k=20. Using this value to determine the maximum of $\varepsilon_{transformation}$ for the dual phase steel, and using the relation as

$$\varepsilon_{plastic} = \varepsilon_{transformation} + \varepsilon_{slip} \tag{35}$$

values of $\varepsilon_{transformation}$ have been estimated ranging from 0.0002 to 0.0028. These values are relatively small compared with the slip strain and so they are considered to have a minor effect on overall transformation behavior. Therefore, the transformational strains can be neglected.

The largest amount of initial transformation within the elastic region can be roughly estimated by using the value of

strain at the elastic limit obtained from the stress-strain curve at 295K and the above equation as $f_v^{\alpha'}=0.022$, corresponding to f=0.25. This implies a different value of $N_v^{\circ\circ}$ from the value obtained in the Cu-Fe system. This value will be estimated in the next section.

5-3. Prediction of Transformation Behavior

The transformation behavior has been estimated by assigning appropriate values to the free-energy change of transformation and the total number of nucleation sites $N_v^{\circ\circ}$ because of uncertainties in estimating the chemical composition and stabilizing effects. Non-linear curve fitting was applied to obtain the set of above values giving the best fit at each temperature, where the mechanical driving force was estimated from the above stress-strain relations and plastic strains. Then, the free energy changes at several temperatures so obtained were compared with the values from Thermocalc.

Fig.20 shows the best fit of experimental data and the resulting values of $\Delta g^{ch}+g_{el}+w_f$ and $N_v^{\circ\circ}$. The initial behavior at different temperatures is fairly well predicted, although discrepancies become larger as the strain increases. Eq.(9) becomes :

$$N_v = 4.0 \times 10^{13} \exp(-0.84\, n_0) + 4.79 \times 10^{20} \left[1 - \exp(-46.0\, \varepsilon^{3.45}) \right] \exp(-3.88\, n_1) \quad (1/m^3)$$

(36)

Fig.21 compares two quantities, $\Delta g^{ch}+g_{el}+w_f$ and Δg^{ch} obtained from Thermocalc. Lines in the figure are linear regressions of both data in terms of absolute temperature. The differences in absolute values are substantial but the slopes are nearly the same. It is to be noted that the transformational entropy changes estimated from two methods showed good agreement.

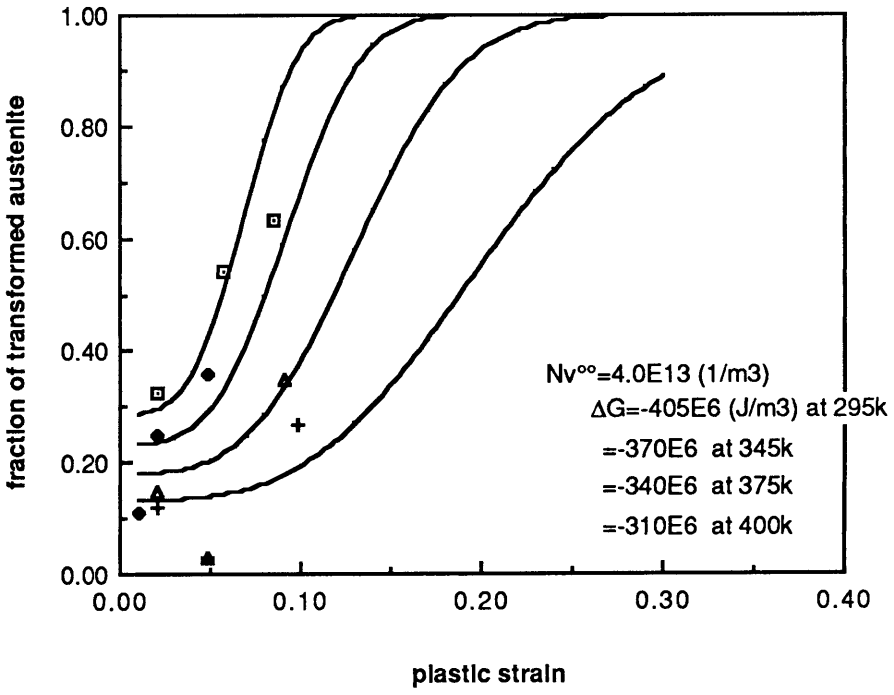

Fig.20 Best fit of the deformation-induced transformation behavior of retained austenite with true plastic strain, using the model and estimating $N_v^{\circ\circ}$ and $DG=g^{ch}+g_{el}+W_f$.

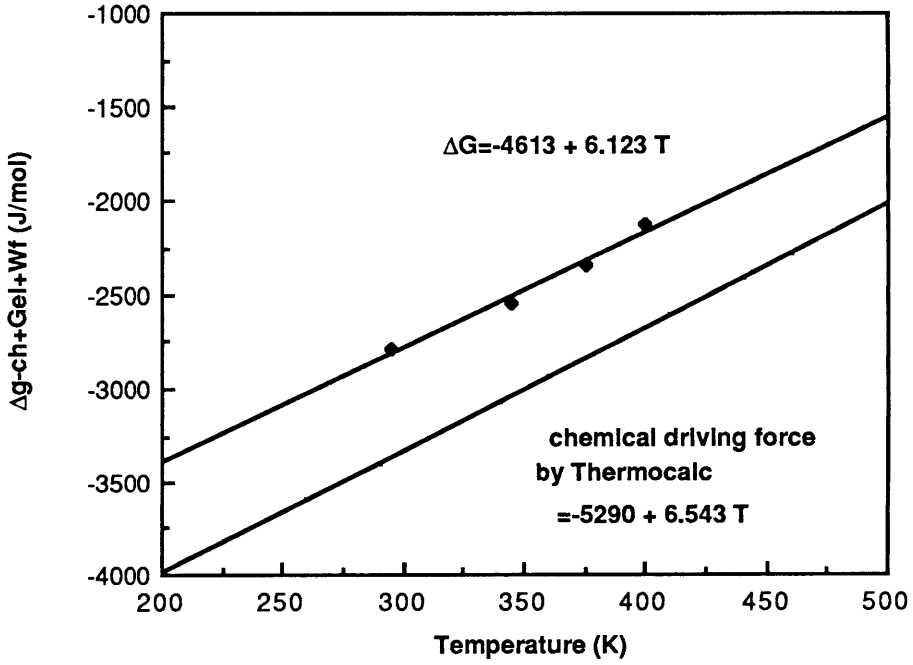

Fig.21 Effects of the chemical composition on austenite stabilization

6. Discussion

6-1. On the Model

A question arises concerning the model develop here as to whether two different distributions of nucleation-site potencies are reasonable. This will be justified by considering a deformation-induced martensitic transformation in a ceramic system.

Chen et al.[17] studied the statistics of stress-assisted martensitic nucleation in ceramics containing zirconia and obtained the change in density of nucleating defects with respect to the excess driving force of transformation. Using the data given by them, values of N_v and number of atomic planes in a nucleation site have been estimated and plotted in Fig.22. From this figure, $N_v^{\circ\circ}$ and α have been obtained as 1.39×10^{16} $(1/m^3)$ and 1.94, respectively. These values imply different distributions of nucleation-site potencies in different systems. In addition to this, taking into account the different mechanism of nucleation, it can be said that stress-assisted and strain-induced nucleation could have different potency distributions.

In order to express the potency distribution for the strain-induced transformation, the large strain dependence of the

total number of nucleation sites of all potencies Nv° has been introduced. This might be attributed to the heterogeneity of slip reported by Fujita et al.[39].

6-2. On the Cu-Fe System

6-2-1. Effect of stress-assisted transformation

The transformation curves for the Cu-Fe alloy is typical of strain-induced nucleation, that is, sigmoidal f vs e curves in the temperature range from 77 to 300K. The number of atomic planes in a nucleating defect has been estimated to be very small. These facts indicate that the austenite in Cu-Fe system is fairly stable in the temperature range studied. Therefore, the effect of stress-assisted nucleation on overall transformation behavior is considered to be very small. The transformational strain will also be very small because of the very small volume fraction of Fe in the alloy.

6-2-2. Prediction of the smallest size of transformed particles

Mori et al. have reported that there is a critical particle size below which strain-induced nucleation will not occur no matter how much a particle is strained. This critical size can be predicted from the model developed here by simply assuming a resolution limit of transformation :

$$d_{critical} = 2\left[\frac{3}{4\pi N_v} \ln\left[\frac{1}{1-f}\right]\right]^{1/3} \quad (m) \tag{37}$$

Assuming two different resolution limits, f=0.01 and f=0.05, the critical particle size is plotted in Fig.23. The good agreement seen in Fig.23 (b) supports the validity of the model.

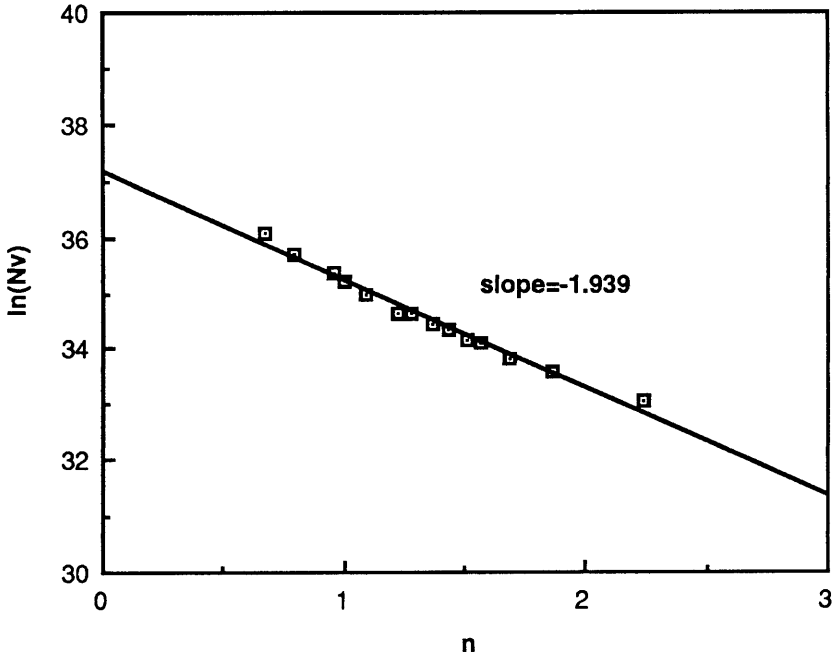

Fig.22 Determinaion of the distribution shape factor for stress-assisted nucleation in the zirconia-containing ceramics

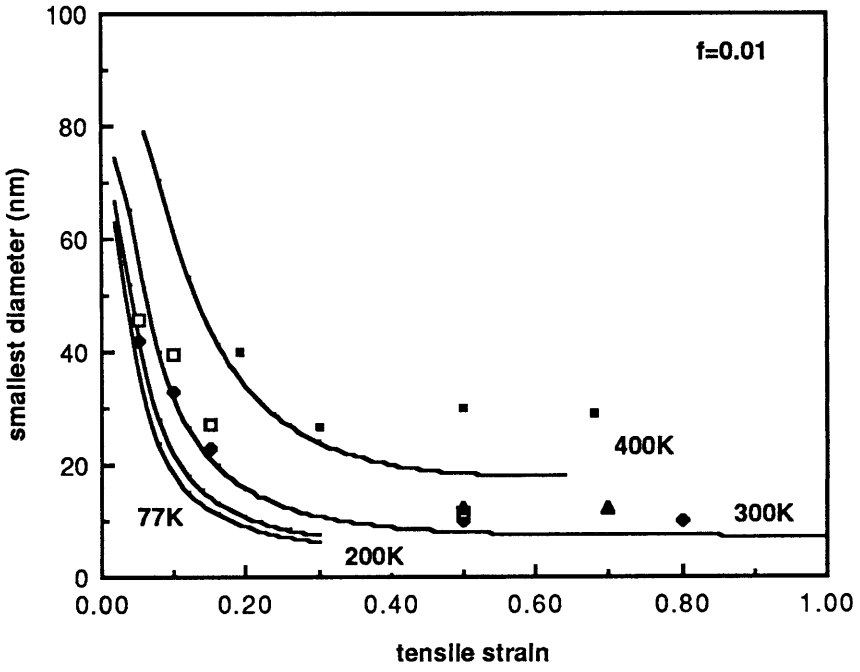

Fig.23-a Comparison of the temperature and strain depenence of the smallest size of transformed particles between experiments and predictions (f=0.01)

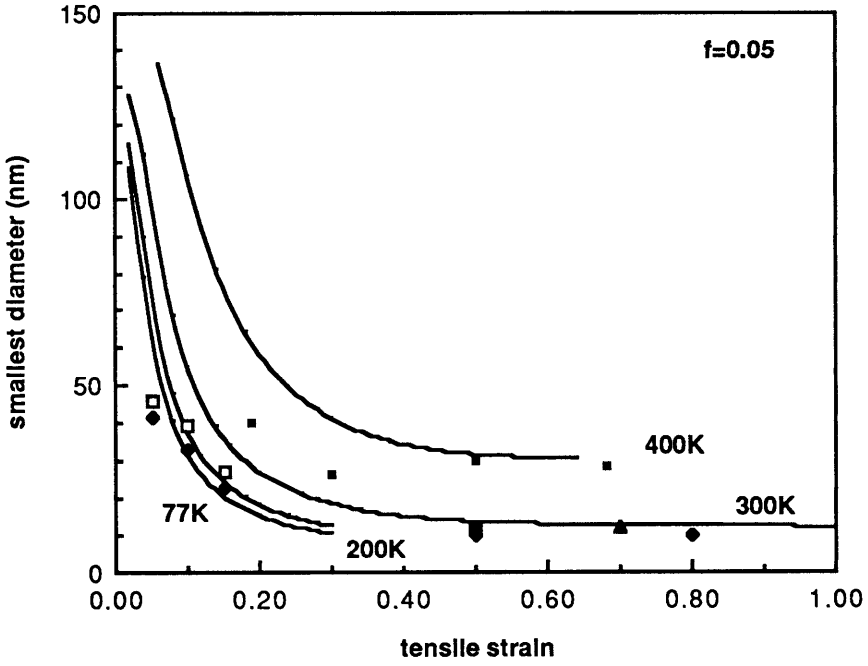

Fig.23-b Comparison of the temperature and strain depenence of the smallest size of transformed particles between experiments and predictions (f=0.05)

6-3. On the Dual-Phase Steel

The difference between $\Delta g^{ch}+g_{el}+w_f$ and Δg^{ch} from Thermocalc observed in Fig.21 is considered to result from the uncertainties in the estimation of both Δg^{ch} and w_f terms. Since the chemical composition of retained austenite has not been well established except for the actually measured Mn content, some errors may be introduced in both term. Among those errors, it can be said from the equation expressing the effect of carbon on w_f that the error due to carbon content might be the largest. Absolute values of both Δg^{ch} and Δw_f will increase as the carbon content increases and this will result in increasing difference between $\Delta g^{ch}+g_{el}+w_f$ and Δg^{ch}. The amount of other elements like Si and N may also introduce some error in the above quantities.

The discrepancy observed in large strain region in Fig.20 may indicate a limitation of this simple model.

7. Conclusions

The kinetics of deformation-induced transformation of dispersed austenite has been studied. A simple model expressing the transformation behavior has been developed based on a previous model for stress-assisted nucleation and assumptions that nuclei have a preferred orientation in strain-induced nucleation. From this study, following conclusions have been drawn :

(1). The mechanical driving force appears to take the maximum value in strain-induced nucleation, different from stress-assisted nucleation.

(2). The potency distribution may have different forms, i.e., different α's in different materials and in different nucleation mechanisms.

(3). The simple model can express the transformation behavior of dispersed austenite in a Cu-Fe single crystal and can predict the change in the smallest size of transformable particles as a function of strain and temperature.

(4). In the case of deformation-induced transformation of retained austenite in a dual-phase steel, the model can account for the contribution of stress-assisted nucleation in the early stage of deformation, but there is increasing discrepancy in the large-strain region.

(5). This discrepancy can be attributed to the simple assumption concerning both the form of the potency distribution for strain-induced nucleation and the form of the total potency distribution.

8. Bibliography

1. V. F. Zackey, E. R. Parker, D. Fahr, and R. Busch, "Enhancement of Ductility in High Strength Steels," Trans. ASM, **7** (1967) pp. 252-259.
2. Tsujimoto, Trans.JIM, **11** (1972) pp. 83.
3. T. Furukawa, H. Morikawa, H. Takechi, and K. Koyama, "Process Factors for Highly Ductile Dual-Phase Steel Sheet," pp. 281-303 in *Structure and Properties of Dual-Phase Steels*, R. A. Kot and J. W. Morris, ed. ; AIME New York, NY, 1979.
4. J. M. Rigsbee and P. J. VanderArend, "Laboratory Studies of Microstructures and Structure-Property Relationship in Dual-Phase Steels," pp. 56-86 in *Formable HSLA and Dual-Phase Steels*, R. A. Kot and J. W. Morris ed. ; AIME, New York, NY, 1979.
5. G. B. Olson and M. Cohen, "A Mechanism for the Strain-Induced Nucleation of Martensitic Transformations," J. Less-Common Metals, **28** (1972) pp.107-118.
6. G. B. Olson and M. Cohen, pp. 1145 , in *Proc. Intl. Conf. Solid-Solid Phase Transf.* (Carnegie-Mellon Univ.) ; AIME, 1982.
7. G. B. Olson and M. Cohen, "Principles of Martensitic Transformations," pp. 43-87, in *Frontiers in Materials Science*, M. A. Meyers and O. T. Inal, ed.; 1985.
8. M. Cohen and G. B. Olson, "Martensitic Nucleation and the Role of Nucleating Defect," pp. 93-98, in *New Aspects of Martensitic Transformation* ; Japan Inst. of Metals, Kobe, Japan, 1977.
9. R. E. Cech and D. Turnbull, " ," Trans. AIME, **206** (1956) pp. 124.
10. G. B. Olson, K. Tsuzaki, and M. Cohen, MIT unpublished research, 1984.
11. K. Tsuzaki and G. B. Olson, MIT unpublished research, 1984.

12. G. B. Olson and M. Cohen, "Kinetics of Strain-Induced Martensitic Nucleation," Met. Trans., **6A** (1975) pp. 791-795.
13. T. Angel, "Formation of Martensite in Austenitic Stainless Steels," J. Iron Steel Inst., **177** (1954) pp.165-174.
14. G. B. Olson and M. Cohen, "A General Mechanism of Martensitic Nucleation: Part I. General Concepts and the FCC-HCP Transformation," Met. Trans., **7A** (1976) pp. 1897-1904.
15. G. B. Olson and M. Cohen, "A General Mechanism of Martensitic Nucleation: Part II. FCC-BCC and Other Martensitic Transformations," Met. Trans., **7A** (1976) pp.1905-1914.
16. I-Wei Chen, Y-H. Chiao, and K. Tsuzaki, "Statistics of Martensitic Nucleation," Acta Met., **33** (1985) pp.1847-1859.
17. J. R. Patel and M. Cohen, "Criterion for Action of Applied Stress in the Martensitic Transformation," Acta Met., **1** (1953) pp. 531-538.
18. K. E. Eastering and H. M. Miekk-oja, "The Martensitic Transformation of Iron Precipitates in a Copper Matrix," Acta Met., **15** (1967) pp.1133-1141.
19. K. E. Eastering and G. C. Weatherly, "On the Nucleation of Martensite in Iron Precipitates," Acta Met., **17** (1969) pp.845-852.
20. K. Matsuura, M. Tsukamoto, and K. Watanabe, "The Work-Hardening of Cu-Fe Alloy Single Crystals containing Iron Precipitates," Acta Met., **21** (1973) pp. 1033-1044.
21. G. R. Woolhouse, "The Mechanical Properties of Cu-1wt.% Fe Single Crystals : An Application of Coherency Strain Control," Phil. Mag., **28** (1973) pp. 65-83.
22. K. R. Kinsman, J. W. Sprys, and R. J. Asaro, "Structure of Martensite in Very Small Iron-Rich Precipitates," Acta Met., **23** (1975) pp.1431-1442.
23. M. Kato, R. Monzen, and T. Mori, "A Stress-Induced Martensitic Transformation of Spherical Iron Particles in a Cu-Fe Alloy," Acta Met., **26** (1978) pp. 605-613.

24. R. Monzen and T. Mori, "Structural Changes of Tron Particles in a Deformed and Annealed Cu-Fe Alloy Single Crystal," Trans. J.I.M., **22** (1981) pp. 65-73.
25. D. K. Bowen and J. W. Christian, "The Calculation of Shear Stress and Shear Strain for Double Glide in Tension and Compression," Phil. Mag., **12** (1965) pp. 369-378.
26. A. K. Sachdev, "Effect of Retained Austenite on the Yielding and Deformation Behavior of a Dual Phase Steel," Acta Met., **31** (1983) pp.2037-2042.
27. T. Ferrence and G. B. Olson, MIT unpublished research, 1986.
28. M. Hillert and M. Waldenstrom, "Isothermal Sections of the Fe-Mn-C System in the Temperature Range 873K-1373K," Calphad, **1** (1977) pp. 97-132.
29. J. B. Gilmour, G. R. Purdy, and J. S. Kirkaldy, "Thermodynamics Controlling the Pro-Eutectoid Ferrite Transformations in Fe-Mn-C Alloys," Met. Trans., **3** (1972) pp.1455-1464.
30. K. Ishida and T. Nishizawa, "Ferrite/Austenite Stabilizing Parameter of Alloying Elements in Steel at 200-500°C," Trans. JIM, **15** (1974) pp.
31. L. Kaufman and H. Bernstein, *Computer Calculation of Phase Diagrams*, Academic Press, 1970.
32. L. Kaufman, "Calculations of Binary Phase Diagrams," *Proc. Intl. Conf. Metallurgical Thermochemistry Fundamentals*, Brunel Univ. and NPL, London, 1971.
33 R. Labusch, "A Statistical Theory of Solid Solution Hardening," J. Phs. Stat. Solid, **41** (1970) pp. 659-669.
34. R. T. Howard, Jr., "The Kinetics of Ausenite-Martensite Decomposition," Sc. D. Thesis, MIT, 1947.
35. K. A. Taylor, "Aging Phenomena in Ferrous Martensites," Sc. D. Thesis, MIT, 1985.
36. L. Kaufman and H. Nesor, "Coupled Phase Diagrams and Thermochemical Data for Transition Metal Binary Systems--IV," Calphad, **2** (1978) pp. 295.
37. L. Kaufman, "Summary of the Proceedings of the Twelfth CALPHAD Meeting," Calphad, **7** (1983) pp.273.

38. G. B. Olson and M. Azrin, "Transformation Behavior of TRIP Steels," Met. Trans., **9A** (1978) pp. 713-721.
39. H. Fujita and S. Kimura, "Role of Conjugate Slip in Deformation of Cu-10at%Al Single Crystals," J. Phs. Soc. Japan, **52** (1983) pp. 157-167.